This is a preprint, the final version is subject to change, of the American Mineralogist (MSA)
Cite as Authors (Year) Title. American Mineralogist, in press.
DOI: https://doi.org/10.2138/am-2020-7174

REVISION 2

Halogens in amphibole and mica from mantle xenoliths: Implications for the halogen distribution and halogen budget of the metasomatized continental lithosphere

Johannes G. Hecker, Michael A.W. Marks*, Thomas Wenzel, Gregor Markl

Department of Geosciences, Eberhard-Karls-Universität Tübingen, Wilhelmstrasse 56, 72074 Tübingen, Germany

* Corresponding author. Email: Michael.marks@uni-tuebingen.de

ABSTRACT

This study reports halogen contents (F and Cl) of amphibole and phlogopite derived from mantle xenoliths and one peridotite massif, for amphibole and phlogopite megacrysts and ultramafic magmatic cumulates (hornblendites) found in alkaline volcanics from 11 localities in Europe and Africa. Amphibole and phlogopite contain more F than Cl with F/Cl ratios

reaching about 160 in phlogopites and 50 in amphiboles. Phlogopites are higher in F (median of 3400 µg/g) than amphibole (median of 1000 µg/g), while median Cl contents are higher in amphibole (290 µg/g) compared to phlogopite (180 µg/g).

The Cl contents and the F/Cl ratios in amphibole and phlogopite from mantle xenoliths exhibit large differences between samples of the same region, recording very large variations of halogen contents in the continental lithosphere. We suggest that the halogen content in such samples largely depends on the initial composition of percolating melts and fluids in the continental lithosphere. During reaction of these agents with peridotitic wall-rocks, Cl is preferentially retained in the fluid as it is much more incompatible compared to water and F. This desiccation effect continuously increases salinity (Cl content) and decreases the F/Cl ratio in the agent with time, causing variable Cl contents and F/Cl ratios in amphibole and phlogopite at a specific locality. Subsequent partial melting processes may then sequester and re-distribute especially Cl among amphibole, phlogopite and melts/fluids as a result of its strong incompatibility, whereas F is much less affected as it behaves slightly compatible. The impact of even small amounts of amphibole and mica on the total halogen budget in the continental lithosphere is significant and both minerals can effectively contribute to the high halogen contents typical of alkaline melts.

INTRODUCTION

The Earth's lithospheric mantle contains significant amounts of halogens (F, Cl, Br and I) with clear differences between different reservoirs (e.g., Klemme and Stalder, 2018; Frezzotti and Ferrando, 2018). The major process for transferring halogens from the Earth's surface into the lithospheric mantle is their transport through subduction zones, either through marine pore fluids or rocks rich in hydrous silicates in the subducted crust or serpentinites (e.g., Rüpke et

al. 2002; Kendrick et al. 2011; 2017; 2018; Barnes et al. 2018; Pagé and Hattori 2019). Eventually, halogens may return to the surface via arc magmatism, which is believed to be important for the heavier halogens (Cl, Br, I), while F is thought to be retained much longer in the subducted slab and, thus, may be transported to greater mantle depths (e.g., Barnes et al. 2018 and references therein). Most of the heavy halogens are released from the subducted slab between the lizardite-antigorite transition and the eclogite facies boundary (e.g., John et al. 2011; Debret et al., 2014). Very shallowly released halogens (at depths of less than 30 km) could even be directly recycled back into the oceanic crust (e.g., Hattori and Guillot 2003; Marschall et al. 2009; Pagé et al. 2016).

Metasomatism in the continental lithosphere may happen through silicate and carbonate melts or through fluids and brines and Selverstone and Sharp (2011) propose three different settings for such metasomatic events: Rift settings, plume settings and subduction settings. Rift and plume settings can result in metasomatic processes through silicate or carbonate melts, whereas subduction zones mostly release fluids and brines that will interact with the overlying mantle wedge. Two major categories of mineral hosts for halogens exist in the continental lithosphere: (i) Volatile-bearing minerals (apatite, amphibole and mica) that formed by metasomatism in the lithospheric mantle (Smith 1981; Smith et al. 1981; Ionov et al. 1997; Klemme and Stalder 2018) and (ii) nominally anhydrous mantle minerals (NAMs), such as olivine, garnet, orthopyroxene and clinopyroxene (e.g., Mosenfelder and Rossman 2013a; Mosenfelder and Rossman 2013b; Grützner et al. 2017; Urann et al. 2017).

The metasomatized continental lithosphere is an important source of alkaline magmas (Pilet et al. 2008; Mayer et al. 2014), which are known to be exceptionally halogen-rich (e.g., Bailey and Hampton 1990; Köhler et al. 2009). Therefore, mantle xenoliths from alkaline magmatic provinces represent the perfect sample type when studying modal mantle metasomatism with respect to halogens and their potential connection to halogen-rich magmatism. For the present

study we investigated amphibole- and phlogopite-bearing mantle rocks and amphibole and phlogopite megacrysts hosted by alkaline igneous rocks. For comparison, we also analysed amphibole from several mafic magmatic cumulates (hornblendites). The data derived from this comprehensive sample set provide insight into halogen storage and redistribution in the continental lithosphere and demonstrate the importance of amphibole and mica for the total halogen budget of the lithospheric mantle and their role as a halogen source for mantle-derived melts.

SAMPLE LOCALITIES

The samples come from 12 localities in Europe and Africa many of which have been studied before (**Fig. 1; Table 1**). In the following, we provide a brief summary of the geological setting of each locality, with the main focus on the volcanic rocks that host the xenoliths and the nature of the samples studied here.

Calatrava (Spain)

The Calatrava volcanic field (CVF) is located around 200 km south of Madrid, where active volcanism took place between 8 and 1.6 Ma and resulted in about 250 volcanic vents, cinder cones and maars (Soto and Giuliani 1979). Volcanism is most likely linked to a continental rift setting and is dominated by melilititic and carbonatitic rocks (López-Ruiz et al. 1993; Bailey et al. 2005). Mantle xenoliths of the CVF comprise spinel lherzolites, wehrlites, dunites, clinopyroxenites and so-called composite xenoliths that show both peridotitic and clinopyroxenitic components (Humphreys et al. 2008; Bianchini et al. 2010; Villaseca et al. 2010; González-Jiménez et al. 2014). For the present study we used each one phlogopite and

amphibole vein in a dunite, one amphibole- and phlogopite-bearing clinopyroxenite and two amphibole megacrysts.

Khibiny (Russia)

The plutonic Khibiny complex is part of the Kola alkaline province and was emplaced between 380 and 360 Ma (e.g., Kramm et al. 1993; Arzamastsev et al. 2007). It mainly consists of ultramafic alkaline rocks, ijolites, melteigites, urtites, nepheline syenites, foyaites and minor carbonatites that are crosscut by numerous dykes and explosion pipes of variable compositions (e.g., Arzamastsev et al. 2013). Mantle xenoliths are mostly found in olivine melanephelinite dykes and explosion pipes. They largely consist of clinopyroxene, phlogopite and amphibole (Arzamastsev et al. 2005); for the present study we used two hornblendites.

Fen (Norway)

The plutonic alkaline-carbonatite Fen complex consists of clinopyroxenites, melteigites, ijolites and carbonatites, with emplacement ages between 523 to 601 Ma. The plutonic rocks are crosscut by ultramafic lamprophyres that have been dated to around 580 Ma (Dahlgren 1994). These lamprophyres occur mainly as dykes and contain spinel lherzolites (Griffin 1973) and up to 10 cm large phlogopite and amphibole megacrysts. It is unclear whether these megacrysts are mantle-derived or represent phenocrysts that crystallized from the lamprophyric melt (Dahlgren 1994). For the present study we used each one phlogopite and amphibole megacryst and two coarse amphibole-phlogopite aggregates.

Oldoinyo Lengai, Eledoi and Labait (Tanzania)

120 The samples from Tanzania originate from three localities in the East African Rift (e.g.,
121 Dawson 1992). It is thought that volcanism in east Africa most likely is of a mantle plume
122 origin (Ebinger and Sleep 1998). (i) Oldoinyo Lengai is the only active volcano erupting
123 carbonatitic lavas. The early stages of the volcano are marked by phonolitic volcanism
124 followed by nephelinitic and natrocarbonatitic eruptions (e.g., Klaudius & Keller 2006).
125 Megacrysts of amphibole and mica are common in the ejecta of Oldoinyo Lengai and we used
126 two amphibole and three phlogopite megacrysts for the present study.

127 (ii) The Eledoi maar is part of the Natron-Engaruka volcanic field southeast of Oldoinyo
128 Lengai. This area features several tuff cones and explosion craters of mostly olivine melilititic
129 and olivine nephelinitic composition (Dawson and Smith 1988). Mantle xenoliths from the
130 Eledoi maar have been described in detail by Dawson and Smith (1988) and Dawson and
131 Smith (1992) and we used two mica-rich clinopyroxenites for the present study. (iii) The
132 Labait cinder cone west of Arusha consists of olivine melilititic tuffs that host abundant and
133 variable mantle xenoliths. The three samples from this locality used in the present study
134 comprise a phlogopite-bearing dunite, a phlogopite vein crosscutting a dunite and a
135 phlogopite-bearing harzburgite. These samples have been petrographically and geochemically
136 characterized in detail before (Rudnick et al. 1993; 1994; Lee and Rudnick 1999).

137

138 **Finero (Italy)**

139 The Finero complex is a peridotite massif that was exhumed during the Alpine orogeny. The
140 complex is subdivided into various units (internal layered unit, amphibole peridotite, external
141 gabbro unit) surrounding a so-called phlogopite peridotite unit (e.g., Giovanardi et al. 2014).
142 The phlogopite peridotite consists of harzburgites and dunites and contains variable amounts
143 of amphibole, clinopyroxene, phlogopite, apatite and carbonates (e.g., Morishita et al. 2003;
144 Morishita et al. 2008; Selverstone and Sharp 2011). Metasomatism occurred most likely as a

result of fluids or melts related to a subduction zone (Hartmann and Wedepohl 1993; Zanetti et al. 1999; Selverstone and Sharp 2011). Amphibole and phlogopite occur either as pockets or veins or, in some parts of the body, as finer grained crystals dispersed in the rock and following a slight foliation. For the present study we sampled two amphibole- and phlogopite-bearing harzburgites and a phlogopite-rich pocket within a harzburgite.

Monte Vulture (Italy)

Monte Vulture is a stratovolcano located around 80 km east of Monte Vesuvius at the southern end of the Apennines. It is part of the intramontane ultra-alkaline province (IUP) where active volcanism can be dated back to the middle Pleistocene (Lavecchia et al. 2002). Volcanism on Monte Vulture took place between 740 and 130 Ka, producing early phonolitic rocks, followed by tephrites, basanites and foidites and rare carbonatitic rocks and ejecta (e.g., Beccaluva et al. 2002; Rosatelli et al. 2000; 2007). Some of the lavas contain abundant mantle xenoliths, partly with abundant carbonate inclusions (Jones et al. 2000; Rosatelli et al. 2007). Further, amphibole and phlogopite megacrysts occur in some lavas (Jones et al. 2000) and we used each two megacrysts of amphibole and phlogopite for the present study.

Eifel (Germany)

The Palaeogene and Quarternary volcanics of the Eifel are part of the Central European volcanic province (CEVP) with more than 300 volcanic centres, the majority being part of the western Eifel (e.g., Schmincke et al. 1983). Volcanism started around 720 Ka ago with predominantly basanitic, nephelinitic, leucitic and tephritic products (e.g., Schmincke 2007). The source of volcanism in the Eifel region is thought to be one or several smaller mantle plumes (Ritter et al. 2001; Keyser et al. 2002). Mantle xenoliths are abundant and variable in composition (Stosch and Seck 1980; Zinngrebe and Foley 1995; Witt-Eickschen et al. 1998;

2003). Based on trace element and isotope data of various mantle xenoliths, at least three different metasomatic events in the continental lithosphere below the Eifel have been proposed (Witt-Eickschen et al. 2003). For the present study we sampled three amphibole- and phlogopite-bearing olivine websterites, one amphibole-bearing harzburgite and a phlogopite megacryst.

Wilcza Góra (Poland)

Wilcza Góra in lower Silesia represents the eastern-most part of the CEVP, with the major lavas having basanitic, alkali basaltic and tephritic compositions (Birkenmajer et al. 2002; 2004). Volcanic activity started around 34 Ma ago, the last recorded activity was dated to 1 Ma (Matusiak-Małek et al. 2017b). Volcanic activity was most likely initiated as the result of a mantle plume and the related Eger graben rift system (Dèzes et al. 2004). Mantle xenoliths are abundant in the basanitic volcanic centres of lower Silesia (Matusiak-Małek et al. 2017a), but Wilcza Góra seems to be the only locality where hydrous phases (mostly amphibole) are more common (Matusiak-Małek et al. 2017b). For the present study we used each one amphibole-bearing lherzolite, harzburgite and wehrlite that have been part of a previous petrographic and geochemical study (Matusiak-Małek et al. 2017b).

Spitsbergen (Norway)

The island of Spitsbergen is the largest island of the Svalbard archipelago located in the Arctic Ocean. Active volcanism occurred in the north-western part of Spitsbergen and is largely confined to three alkali olivine basaltic to nephelinitic centres: the Sverrefjell volcano (100 – 250 Ka), and the Halvdanpiggen Sigurdfjell diatremes and slag cones (Griffin et al. 2012). Some of the lava flows consist of up to 70 % of mantle and lower crustal xenoliths (Amundsen et al. 1987; Griffin et al. 2012). For the present study we used two amphibole-

bearing websterites and one hornblendite, previously characterized by Goncharov et al. (2015).

ANALYTICAL METHODS

Electron microprobe (EPMA)

The compositions of amphiboles and micas have been determined using a JEOL Superprobe JXA-8900RL electron microprobe at the department of Geosciences, University of Tübingen. The wavelength dispersive mode (WDS) was used, applying an acceleration voltage of 15 kV and a beam current of 20 nA. Calibration was done using natural and synthetic standards, counting times were 16 s for major elements (Si,Ti, Al, Ca,Mg, Fe, Mn, Na, K) and 30 s for minor elements (Ba, Cr) on the peak position and 8 s and 15 s on the background positions, respectively. A beam diameter of 5 µm was used to minimize migration of alkalis and volatiles. Data reduction was performed using the internal Φρz matrix correction of JEOL (Armstrong 1991). For the analysis of F and Cl, we used a LDE1 and PETH crystal, respectively, with counting times of 30 s on the peak position and 15 s on both background positions. This protocol resulted in average detection limits of about 250 µg/g for F and about 40 µg/g for Cl. Due to a peak overlap between the F $K\alpha_1$ signal with the Fe $L\alpha_{1,2}$ and the adjacent Al $K\alpha_{1,2}$ and Mg $K\alpha_{1,2}$ and various Mg $SK\alpha_{1,2}$ and lines caused by the relatively low resolution of the LDE crystal, a manual adjustment of the upper and lower backgrounds was necessary. Several amphibole and mica crystals with varying FeO and Al_2O_3 contents were analysed to make sure the corrected background positions fit to all amphiboles and micas with

variable compositions. Overlap correction was done by measuring a natural F-free hematite standard and then correct the apparent F counts to 0. Due to this correction procedure, the analytical uncertainty is estimated to 15-20 % for F measurements, the analytical uncertainty for Cl is about 10 %. The long-term reproducibility of the measurements was checked by periodically re-analyzing the used standards (topaz and tugtupite, respectively) and monitoring their agreement with certified standard values during each analytical session. The resulting k-ratios were between 0.99 and 1.01. Also, we re-analyzed some of the samples during different analytical sessions and found no differences exceeding the mentioned uncertainties.

PETROGRAPHY

The modal composition of the studied samples and the textural appearance of amphibole and mica in these samples vary greatly (**Table 1**). In some samples, amphibole and/or mica are in textural equilibrium with the surrounding matrix of olivine (ol), orthopyroxene (opx), clinopyroxene (cpx) and spinel (spl), while in others, they show clear reaction and disequilibrium textures, partly replacing former ol, cpx and spl (see below). In very few cases, amphibole and mica grew alongside smaller cracks in the xenolith towards the surrounding volcanic rock, probably because of interaction with the host magma during ascent/transport of the xenolith. Such textures are not the topic of this study and are not considered further here. In the following, we distinguish two types of mantle xenoliths based on their modal mineralogy:

Type I: Dunites, harzburgites, lherzolites and wehrlites

These samples are ol-rich with minor opx, cpx, spinel, amphibole and mica, resembling group I xenoliths according to the classification of Frey and Prinz (1978). These samples have experienced variable metasomatic events resulting in the formation of cpx, amphibole and mica. In most of these samples, the metasomatic phases are in textural equilibrium with the matrix minerals (e.g. in samples from Finero (FIN-01), Wilcza Góra (WLK30, MLK33 & MM110), Eifel (EIF-09) and Labait (LB-33); **Figs. 2a and b**). Some samples from Calatrava (14649 & 100002) contain amphibole- and mica-rich veins crosscutting the ol-rich matrix (**Fig. 2c**). Textural equilibrium between cpx and amphibole in samples from Wilcza Góra (WLK30 & MM110) indicate their simultaneous growth during the same metasomatic event. In some cases, amphibole is surrounded by fine-grained rims of ol, cpx and spl (**Fig. 2d**), which has been interpreted as resulting from breakdown reactions of amphibole during ascent of the xenolith to the surface (Ban et al. 2005).

Type II: Clinopyroxenites, websterites and olivine websterites

These samples are dominated by cpx and opx, with variable amounts of ol, amphibole and mica resembling group II xenoliths sensu Frey and Prinz (1978). Samples of this group comprise EIF-02, -04 & -08 (Eifel), ELD-2009-06-1 & -06-2 (Eledoi), 120091 (Calatrava), SHP-10 &-26 (Spitsbergen). Pervasive metasomatism crucially changed the modal composition of these rocks and various reaction and replacement textures are common in these samples: samples from the Eifel (EIF-02, -04 & -08) show variable replacement of ol and cpx by amphibole and mica, with the latter two often being intergrown with each other, indicating concurrent growth (**Fig. 2e**). Samples from Eledoi (ELD-2009-06-1 & -06-2) show equilibration of mica with cpx (**Fig. 2f**). In samples from Calatrava (120091) and Spitsbergen

(SHP-26), cpx is partly replaced by amphibole and mica, indicating that metasomatic growth of cpx happened prior to the growth of amphibole and phlogopite.

Megacrysts

Megacrysts have been studied from five localities (Calatrava, Oldoinyo Lengai, Monte Vulture, Fen, Eifel) and comprise several cm-sized single crystals of either mica or amphibole typically found as loose crystals in volcanic rocks and tuffs. A mantle origin for such megacrysts is generally assumed, one possible source being amphibole- and phlogopite-rich veins and pockets in the lithospheric mantle (Dawson and Smith 1982). However, as the textural relation is obscured, it is in fact possible that they simply crystallized from the magma by which they were transported to the surface.

Hornblendites

For comparison hornblendites from Spitsbergen and Khibiny have been studied. They show typical cumulate textures with coarse-grained amphibole and variable amounts of mica, cpx, apatite and magnetite, partly enclosed in amphibole (**Figs. 2g and 2h**).

RESULTS

Mineral chemistry (EPMA)

Mica. Mineral formula calculations for mica are based on 22 oxygen atoms and exemplary EPMA analyses of micas are given in **Table 3**. All micas (N=174) are phlogopites with Mg numbers (Mg# = Mg/(Mg+Fe_{tot})) ranging from 0.70 to 0.95 (**Fig. 3**). The Mg#, SiO_2 and TiO_2 contents (wt.%) of phlogopites from type I and II samples largely overlap with each other and with megacrystic phlogopite and phlogopite from hornblendites (**Fig. 3a and b**). The Cr_2O_3 contents in mica from type I and II samples reach up to 2.6 wt.% Cr_2O_3, while Cr_2O_3 contents in phlogopite megacrysts and phlogopite from hornblendites are always <1 wt.% (**Fig. 3c**).

Fluorine contents mostly range between 0.12 and 0.87 wt.% (median of 0.34 wt.%), but exceptionally high F (up to 3.1 wt.%) was detected in phlogopite from a dunite from Tanzania (**Fig. 4a**). Chlorine contents are mostly below 600 µg/g (median of 180 µg/g) with about 10 % of the analyses being below the detection limit (about 40 µg/g; **Table 2**). Exceptionally high Cl (800-1100 µg/g) was detected in phlogopite from a harzburgite from Finero (**Fig. 4a**). Halogen contents of megacrystic phlogopites and phlogopite from hornblendites largely overlap with those from mantle xenoliths (**Fig. 4a**). The F/Cl ratios are highly variable, ranging from about 1 (Finero) to 160 (Tanzania). There are no general and no sample specific negative correlations of X_{Cl} with Mg# or X_F with Fe# (**Figs. 4b and c**), as could be expected because of crystal chemical effects concerning the incorporation of Cl and F (Munoz 1984; Volfinger et al. 1985; Leger et al. 1996).

Amphibole. Formula calculations for amphiboles are done using the Excel spreadsheet of Locock (2014), based on the current IMA nomenclature (Hawthorne et al. 2012). Exemplary EPMA analyses are given in **Table 4**. The major element composition of all amphiboles (N=214) falls within the known range of mantle amphiboles (e.g. Coltorti et al. 2007) indicating mostly pargasitic and hastingsitic compositions with Mg# between 0.60 and 0.91

(**Fig. 5a**). The Mg# and SiO_2 and TiO_2 contents (wt.%) largely overlap between types I and II, megacrysts and hornblendites (**Fig. 5b**).

Fluorine contents in amphiboles are generally lower than in phlogopites. About 15 % of the analyses are below the EPMA detection limit (about 250 µg/g; **Table 2**). Most analyses are below 2000 µg/g with a median value of about 1000 µg/g (**Fig. 6a**). Some of the highest F contents (up to 5000 µg/g F) were detected in megacrystic amphibole from Oldoinyo Lengai and Mont Vulture (**Fig. 6a**). Chlorine contents are mostly below 600 µg/g (median of 290 µg/g) but reach about 1100 µg/g (Fig. 6a). Importantly, Cl contents in amphibole from different samples of the same region are highly variable: amphibole from the Finero phlogopite-harzburgite contains up to 1000 µg/g Cl, whereas amphibole from the Finero amphibole-peridotite reaches only 90 µg/g Cl. Similarly, amphibole in a sample from Dreiser Weiher, (Eifel) is much higher in Cl (up to 1000 µg/g) compared to other samples from the Eifel, with maximum values of about 320 µg/g Cl (**Fig. 6**). As for phlogopites, samples from individual regions show no correlation between X_F and Fe# or X_{Cl} and Mg#; in fact, the highest Cl concentrations are reached in amphiboles with the highest Mg# **(Figs. 6 b and c)**. Positive correlations between K and X_F as described by Volfinger et al. (1985) are also missing, but variations in Fe, Mg and K are generally low within samples from the same region.

DISCUSSION

Comparison with existing halogen data for mantle-derived amphibole and phlogopite

Although major and trace element data for mantle-derived amphibole and phlogopite are abundant in the literature, only few studies include halogen data as well (e.g. Chalot-Prat and Boullier 1997; Coltorti et al. 2004). A recent summary of literature data on halogens in mantle-derived amphibole and phlogopite is given in Klemme and Stalder (2018). While our amphibole data largely overlap with literature data, a larger proportion of our phlogopite data show considerably lower Cl and F compared to literature data (**Fig. 7**). Note that most of the literature data represent phlogopite from kimberlitic rocks and such phlogopites are known for their elevated F concentrations that are not well understood (e.g. Reguir et al. 2009). In contrast, phlogopite from lherzolite xenoliths within kimberlites is notably lower in F (Giuliani et al. 2016), overlapping well with our data (**Fig. 7**).

Literature phlogopite data of the Finero phlogopite harzburgite (mean values of 300 µg/g Cl; Exley et al. 1982; Haclick 2010) are not in accordance with our data that show highly variable Cl contents (up to 1100 µg/g in FIN-01 and around 60 µg/g in FIN-02; **Fig. 4**). We suggest that these large differences between samples reflect local variations in halogen contents in the mantle (discussed further below). Large halogen variations have been reported for amphiboles from sub-arc mantle xenoliths from Kamchatka, Russia (Bénard et al. 2017), ranging in F from 500 to 5500 µg/g, similar to the range of our data (**Fig. 7**). Chlorine contents in these amphiboles, however, are much lower than in most amphiboles from our study.

Formation conditions of amphibole and phlogopite and their metasomatic agents

Correlating the textures of amphibole and phlogopite in mantle xenoliths with different metasomatic agents is not a simple task, as it is not easy to decide if these minerals formed because of interaction with melts or fluid or both based on textures alone and even major and trace element data can often not clarify the nature of metasomatic agents in the mantle beyond

363 doubt (e.g., Ionov et al. 2002). Nevertheless, some previous studies provide further
364 information (Witt-Eickschen et al. 1998; 2003; Gervasoni et al. 2017; Matusiak-Małek et al.
365 2017b), making it possible to draw some conclusions on the metasomatizing agents that cause
366 the formation of amphibole and phlogopite.

367 In type I xenoliths (dunites, harzburgites, lherzolites and wehrlites) amphibole and phlogopite
368 are typically dispersed in the samples and not restricted to, or more abundant at, the rims of
369 the xenoliths. Hence, amphibole and phlogopite formed due to metasomatism in the mantle
370 and did not grow because of interaction with the host magma that transported the xenoliths to
371 the surface. In samples from Poland (WLK30 and MM110), cpx is not in textural equilibrium
372 with ol but is intergrown with amphibole, which indicates that amphibole and cpx formed
373 during the same metasomatic event. Based on the presence of amphibole and phlogopite and
374 geochemical indicators (e.g., high $(La/Yb)_N$ and Ti/Eu ratios) as well as high oxygen fugacity,
375 a hydrous silicate-carbonate melt was proposed as the metasomatic agent (Matusiak-Małek et
376 al. 2017b).

377 Type II xenoliths (clinopyroxenites, websterites and olivine-websterites) are cpx-rich and
378 contain abundant amphibole and phlogopite, while ol is often replaced (see above). The
379 formation of such rocks may occur in mafic magma chambers via fractional crystallisation, as
380 a metasomatic reaction between peridotite and hydrous silicate or carbonatite melts, or as
381 segregations and melts from the peridotites themselves (Sinigoi et al. 1983; Pearson et al.
382 1993; van Acken et al. 2010; Gervasoni et al. 2017). As no cumulate textures are present in
383 the studied samples, we suggest that our samples represent reaction-type clinopyroxenites,
384 most likely caused by hydrous silicate melts (possibly with a carbonate component) that
385 reacted with the peridotite wall rock. In fact, reaction-type experiments between peridotite
386 and hydrous silicate melts resulted in the growth of amphibole-rich layers on partly reacted
387 peridotite (Gervasoni et al. 2017). In some of our samples, abundant amphibole and

388 phlogopite and cpx imply high melt/rock ratios or long reaction times with the initial
389 peridotite, similar to the formation of amphibole- and phlogopite-rich veins that formed from
390 melts percolating through the mantle (e.g., Witt-Eickschen et al. 1998). Such vein-type
391 textures were observed in samples from Calatrava (14649 and 10002; **Fig. 2c**). Similar
392 reaction experiments between peridotite with carbonatite resulted in abundant replacement of
393 opx by cpx resembling the transformation to a wehrlite (Gervasoni et al. 2017).

394 The formation conditions of amphibole and phlogopite megacrysts are uncertain due to the
395 missing textural context. They have been related to vein-type amphiboles and phlogopites
396 (Dawson and Smith 1982; Bodinier et al. 1987; Shaw and Eyzaguirre 2000) although their
397 composition clearly overlaps with type I and II mantle xenoliths (**Figs. 3 and 5**).
398 Alternatively, they could resemble disaggregated magmatic cumulates or could represent
399 phenocrysts of the rock in which they are found (see above). Given the compositional overlap
400 with xenolith-hosted amphibole in this study (**Figs. 3 and 5**) we consider a phenocryst origin
401 of the samples unlikely. Yet, the compositional variability is quite large and thus, an origin
402 from different reservoirs for the individual samples cannot be excluded. Consequently, these
403 samples are not discussed further.

404 Hornblendites probably resemble magmatic cumulates based on their textures (**Figs. 2g and**
405 **2h)**. These rocks crystallized from rather hydrous magmas in the (lower) crust. In that sense,
406 they are not related to type I and II mantle xenoliths but it is important to stress that based on
407 their major element chemistry and halogen contents, they cannot be distinguished. These
408 samples are also excluded from further discussion.

409

410

411 **Controls of F and Cl incorporation into amphibole and phlogopite**

The experimentally derived so-called Fe-F and Mg-Cl avoidance rules (e.g. Munoz 1984; Volfinger et al. 1985; Leger et al. 1996) suggest that under equilibrium conditions, mica and amphibole from individual samples should show positive correlations between Mg and F and negative ones between Fe and F. Such effects are not obvious in the investigated samples (**Figs. 4b, c and 6b, c**), which is probably because of relatively small variations of Mg and Fe in individual samples. Note that the apparent positive correlations between Cl/(Cl+OH+F) and X_{Mg} (**Figs. 4c and 6c**) and a negative one between F/(F+Cl+OH) and XFe (**Fig. 4b**) among all samples are defined by exceptionally F- and Cl-rich samples. After all, a "global trend" among all samples is not expected anyway.

We suggest that the relatively large variations in halogen contents in individual samples (**Figs. 4a and 6a**) are mostly governed by the nature and composition of the metasomatic agents from which they crystallized, as suggested by Smith et al. (1981). Melts/fluids that percolate through peridotite will change (not only) their halogen composition during interaction and may cause formation of amphibole and mica, if water activity is high enough. The formation of amphibole and phlogopite instead of NAMs consumes water and the salinity of the remaining fluid increases, causing desiccation. Due to strong incompatibility of Cl in amphibole and phlogopite (D values < 0.1; e.g., Van den Bleeken and Koga 2015; Bénard et al. 2017), Cl will preferably stay in the fluid phase. While the amount of fluid will largely decrease (because of the formation of hydrous silicates), Cl may be enriched to the wt.% level in the evolving fluid culminating in the formation of highly saline brines (e. g., Markl and Bucher, 1998; Kusebauch et al., 2015). Additionally, experimental data imply that NAMs can sequester some H_2O, but much less Cl, as D(Cl) << D(H) and the maximum Cl solubility for NAMs is very low (2.1 – 11.4 ppm) and independent of the fluid salinity (0.3-30 wt.% Cl; Bernini et al., 2013). Although no such study has been conducted on natural mantle rocks, it is most likely that desiccation plays a fundamental role for fluids and melts percolating through the upper mantle. We suggest that variable Cl contents in amphibole and phlogopite

438 from several type I samples of the same region indicate such a process. Mineral-fluid partition
439 coefficients for F are 1-2 orders of magnitude larger than for Cl and F seems to be slightly
440 compatible in amphibole under mantle conditions (D values of about 1-4; Bénard et al. 2017;
441 Van den Bleeken and Koga 2015). Therefore, the desiccation effect causes decreasing F/Cl
442 ratios in hydrous silicates with increasing fluid consumption and Cl enrichment (**Fig. 8**).

443

444

445 **Distribution and recycling of halogens in the lithosphere**

446 Large amounts of halogens enter the lithospheric mantle through subduction zones (O'Reilly
447 and Griffin 2000; Kendrick et al. 2014; Pagé and Hattori 2019). The primary source for Cl
448 seems to be the serpentinites, whereas F is more likely to originate from crustal sediments,
449 gabbros and rocks affected by e. g. black smokers, where magmatic fluids play a significant
450 role (Orberger et al. 1999; Debret et al. 2014; Pagé and Hattori 2017). The release of halogen-
451 bearing fluids from the subducted slab will cause metasomatic reactions with the peridotite
452 wall-rock, and the halogens will be distributed between newly formed apatite, amphibole, and
453 phlogopite and NAMs (e.g., Ionov et al. 1997; O'Reilly and Griffin 2000; Beyer et al. 2012;
454 Urann et al. 2017). Because the Finero complex is thought to be a mantle wedge that has been
455 metasomatized by subduction zone fluids or melts (Zanetti et al. 1999), one can assume that
456 this first step can produce high Cl contents in amphibole and phlogopite, as F is believed to be
457 retained much longer in the subducted slab and, thus, may be transported to greater mantle
458 depths (e.g., Barnes et al. 2018 and references therein). Indeed, harzburgites from Finero
459 (FIN-01) show the highest Cl concentrations in amphibole and phlogopite **(Figs. 4 and 6**).

460 Clinopyroxenites and websterites (type II xenoliths) most likely experienced metasomatic
461 overprint through hydrous silicate or carbonate melts that are not necessarily related to
462 subduction zone processes (see above). Halogens in such melts mainly derive from partial

463 melting of NAMs (e.g., Urann et al., 2017), although melting of pre-existing halogen-bearing
464 minerals originating from ancient subduction zone metasomatism may have contributed to the
465 halogen budget of such melts to a certain amount as well. Mixing of these two halogen
466 reservoirs (NAMs and ancient subduction-related amphibole, phlogopite and apatite) will
467 likely result in generally lower halogen contents in such melts compared to subduction zone
468 fluids. Therefore, Cl contents in amphibole and phlogopite grown as a result of metasomatic
469 events unrelated to subduction zone processes (c.f. those related to plume or rift settings) are
470 expected to be lower in Cl than those that have initially grown as a result of fluid-induced
471 metasomatism above subduction zones. Such differences can be detected between type I and
472 type II samples from the Eifel, where a (type I) harzburgite (EIF-09) contains much more
473 amphibole that is considerably higher in Cl (arround 1000 μg/g) than in (type II) websterites
474 (EIF-02 and 04) from the Weinfelder Maar (100-300 μg/g; **Fig. 6a**). Consequently, halogen
475 contents in Eifel xenoliths would originate from two different metasomatic events, one being
476 subduction-related (EIF-09), the other being related to mantle upwelling during a rift or plume
477 setting (EIF-02 and 04). This is in accordance with earlier evidence for different metasomatic
478 events that affected the mantle beneath the Eifel (Witt-Eickschen et al. 2003) and large-scale
479 metasomatic effects of the mantle beneath Europe caused by subduction during the Variscan
480 orogeny (Kroner and Romer 2013).

481 In all, a generally low input of Cl into the upper mantle (due to its early loss during
482 subduction) and the easy possibility of Cl to leave the mantle through melts, most likely
483 accounts for the lower Cl concentrations compared to F in amphibole and phlogopite. In
484 contrast, F is preferably retained in subducting slabs (Straub and Layne 2003; Pagé and
485 Hattori 2019) and is stable in volatile-bearing minerals until great depths, making it possible
486 to enrich the upper mantle in F (Pagé and Hattori 2017). Thus, the F/Cl ratio of the mantle
487 may increase with depth (Wysoczanski et al. 2006), and is further influenced by melt
488 extraction.

489

490 **Amphibole and phlogopite as halogen sources in the continental lithosphere**

491 Recent studies revealed halogen concentrations in NAMs generally at the low to sub µg/g
492 level (e.g., Beyer et al. 2012; Urann et al. 2017). However, due to their higher abundance
493 compared to amphibole and mica, large parts of the halogen content of the mantle may be
494 stored in olivine, garnet, orthopyroxene and clinopyroxene (Beyer et al. 2012; Grützner et al.
495 2017). Nevertheless, as implied by the mantle xenolith record, halogen-bearing minerals
496 (apatite, amphibole, mica) are locally abundant, at least in the continental lithosphere and
497 their occurrence may be widely underestimated (O'Reilly and Griffin 2000).

498 Whether amphibole and mica contribute significantly to the halogen budget of the continental
499 lithosphere can be investigated by exemplary mass-balance calculations (**Table 5)**. For these
500 estimates, we assume a hypothetical peridotite consisting of 60 wt.% olivine, 20 wt.% opx
501 and 20 wt.% cpx. The halogen (F and Cl) content of this model peridotite was then calculated
502 using published F and Cl contents for NAMs from natural lherzolites and harzburgites (Urann
503 et al. 2017; resembling type I xenoliths of our study). The data presented by Urann et al.
504 (2017) report F and Cl contents of olivine (11 grains), orthopyroxene (15 grains) and
505 clinopyroxene (15 grains) from 17 natural peridotite samples that originate from a variety of
506 tectonic environments including supra-subduction ophiolites, subduction-metasomatized
507 subcontinental lithospheric mantle, un-metasomatized subcontinental lithospheric mantle,
508 metasomatized mantle-derived xenoliths and fresh abyssal peridotites from the Mid Atlantic
509 Ridge spreading center. Using mean F and Cl concentrations for olivine (6.1 and 0.23 µg/g),
510 opx (6.9 and 0.23 µg/g) and cpx (22.1 and 0.25 µg/g) results in 9.5 µg/g F and 0.23 µg/g Cl
511 for the assumed model peridotite (**Table 5**). We compare these data with median F and Cl
512 contents for amphibole (1020 and 630 µg/g) and phlogopite (3890 and 450 µg/g) from type I
513 xenoliths of our study (**Fig. 7)**. As expected, the impact of small amounts of amphibole and

514 mica on the total halogen budget of the model lherzolite is very large (**Fig. 9**). Especially Cl
515 content is largely controlled by amphibole and phlogopite, because of the very low Cl
516 contents in NAMs from natural peridotite samples (**Table 5**). If 1 % of the lherzolite consists
517 of amphibole and/or phlogopite, this amounts for >90 % of the total Cl budget. The influence
518 on the total F budget is lower (50-80% of the total F), but still significant (**Fig. 9**). Note that
519 this simplified model does not take into account potential mineralogical (and geochemical)
520 variations expected for different mantle lithologies. However, given the very low halogen
521 contents and the limited variation found in NAMs so far, especially for Cl (**Table 5**),
522 calculations reflecting different geodynamic settings (e.g., metasomatized continental
523 lithosphere, sub-arc mantle, OIB-source mantle) would produce basically identical results.

524

525

526 **IMPLICATIONS**

527 The halogen concentration in amphibole and phlogopite from mantle xenoliths depend on: (i)
528 The compositional evolution of metasomatic fluids/melt, as the reaction between peridotite
529 wall rock and metasomatizing agent may cause a desiccation effect, which increases the Cl
530 content and decreases the F/Cl ratio in the agent from which amphibole and phlogopite may
531 form with time. (ii) Partial melting events after amphibole and phlogopite formation, as these
532 will decrease the halogen contents and increase the F/Cl ratios of amphibole and mica.

533 The impact of even small amounts of amphibole and mica on the total halogen budget in the
534 continental lithosphere is significant and especially the Cl budget may be largely controlled
535 by amphibole and phlogopite. Given the strongly incompatible behaviour of Cl during partial
536 melting, amphibole and phlogopite can be considered to be of major importance for the Cl
537 budget of low-degree partial melts derived from the mantle, with a less pronounced effect for
538 F. Alkaline magmas are known to be exceptionally rich in halogens, reaching wt.% levels of

539 F and Cl in evolved magmas. This probably reflects the combined effects of (i) initially
540 halogen-rich and low-degree partial melts derived from amphibole- and phlogopite-bearing
541 mantle domains and (ii) further enrichment of halogens via subsequent magmatic
542 differentiation and retention of halogens. In order to quantify the impact of amphibole and
543 phlogopite melting on the halogen budget of mantle-derived melts, dedicated experimental
544 work on this problem is warranted.

545

546

547 **ACKNOWLEDGMENTS**

548 We are grateful to (in alphabetical order) Andrej Arzamastsev, Sven Dahlgren, Attila
549 Demény, Alexey Goncharov, Emma Humphreys-Williams, Jurgis Klaudius, Anreas Klügel,
550 Magdalena Matusiak-Malek, Gianluigi Rosatelli, Roberta Rudnick, and Anatoly Zaitsev for
551 kindly providing sample material for this study and shared their detailed knowledge on the
552 studied localities. We further thank David Günzler for hand-picking of sample material and
553 Simone Schafflick for preparing thin sections and sample mounts. We further acknowledge
554 the comments of two anonymous reviewers and the editorial handling of Anita Cadoux.

555

556

557 **REFERENCES CITED**

558 Amundsen, H., Griffin, W., O'Reilly, S.Y. (1987) The lower crust and upper mantle beneath
559 northwestern Spitsbergen: evidence from xenoliths and geophysics. Tectonophysics, 139,
560 169-185.

561 Armstrong, J.T. (1991) Quantitative elemental analysis of individual microparticles with electron
562 beam instruments Electron probe quantitation. Springer, pp 261-315.

563 Arzamastsev, A., Belyatsky, B., Travin, A., Arzamastseva, L., Tsarev S. (2005) Dike rocks in the
564 Khibina Massif: relations with the plutonic series, age, and characteristics of the mantle
565 source. Petrology, 13, 267-288.

566 Arzamastsev, A., Arzamastseva, L., Travin, A., Belyatsky, B., Shamatrina, A., Antonov, A.,
567 Larionov, A., Rodionov, N., Sergeev S. (2007) Duration of formation of magmatic system
568 of polyphase Paleozoic alkaline complexes of the central Kola: U-Pb, Rb-Sr, Ar-Ar data
569 Doklady Earth Sciences. Springer, pp 432-436.

570 Arzamastsev, A.A., Arzamastseva, L.V., Zhirova, A.M., Glazne,v V.N. (2013) Model of
571 formation of the Khibiny-Lovozero ore-bearing volcanic-plutonic complex. Geology of
572 Ore Deposits, 55, 341-356.

573 Bailey, D., Hampton, C. (1990) Volatiles in alkaline magmatism. Lithos, 26, 157-165.

574 Bailey, K., Garson, M., Kearns, S., Velasco, A. (2005) Carbonate volcanism in Calatrava, central
575 Spain: A report on the initial findings. Mineralogical Magazine, 69, 907-915.

576 Ban, M., Witt-Eickschen, G., Klein, M., Seck, H. (2005) The origin of glasses in hydrous mantle
577 xenoliths from the West Eifel, Germany: Incongruent break down of amphibole.
578 Contributions to Mineralogy Petrology, 148, 511-523.

579 Barnes, J.D., Manning, C.E., Scambelluri, M., Selverstone, J. (2018) The behavior of halogens
580 during subduction-zone processes. The Role of Halogens in Terrestrial and Extraterrestrial
581 Geochemical Processes. Springer, pp 545-590.

582 Beccaluva, L., Coltorti, M., Di Girolamo, P., Melluso, L., Milani, L., Morra, V., Siena, F. (2002)
583 Petrogenesis and evolution of Mt. Vulture alkaline volcanism (Southern Italy). Mineralogy
584 Petrology, 74, 277-297.

585 Bénard, A., Koga, K., Shimizu, N., Kendrick, M., Ionov, D., Nebel, O., Arculus, R. (2017)
586 Chlorine and fluorine partition coefficients and abundances in sub-arc mantle xenoliths

(Kamchatka, Russia): Implications for melt generation and volatile recycling processes in subduction zones. Geochimica et Cosmochimica Acta, 199, 324-350.

Bernini, D., Wiedenbeck, M., Dolejš, D., Keppler, H. (2013) Partitioning of halogens between mantle minerals and aqueous fluids, implications for the fluid flow regime in subduction zones. Contributions to Mineralogy Petrology, 165, 117-128.

Beyer, C., Klemme ,S., Wiedenbeck, M., Stracke, A., Vollmer, C. (2012) Fluorine in nominally fluorine-free mantle minerals: experimental partitioning of F between olivine, orthopyroxene and silicate melts with implications for magmatic processes. Earth Planetary Science Letters, 337, 1-9.

Bianchini, G., Beccaluva, L., Bonadiman, C., Nowell, G.M., Pearson, D.G., Siena, F., Wilson, M. (2010) Mantle metasomatism by melts of HIMU piclogite components: new insights from Fe-lherzolite xenoliths (Calatrava Volcanic District, central Spain). Geological Society, London, Special Publications, 337, 107-124.

Birkenmajer, K., Pécskay, Z., Grabowski, J., Lorenc, M.W., Zagożdżon, P.P. (2002) Radiometric dating of the Tertiary volcanics in Lower Silesia, Poland. III. K-Ar and palaeomagnetic data from Early Miocene basaltic volcanics near Jawor, Fore-Sudetic Block Annales Societatis Geologorum Poloniae. pp 241-253.

Birkenmajer, K., Pécskay, Z., Grabowski, J., Lorenc, M.W., Zagożdżon, P.P. (2004) Radiometric dating of the Tertiary volcanics in Lower Silesia, Poland. IV. Further K-Ar and palaeomagnetic data from Late Oligocene to Early Miocene basaltic rocksof the Fore-Sudetic Block Annales Societatis Geologorum Poloniae. pp 1-19.

Bodinier, J.-L., Fabriès, J., Lorand, J.-P., Dostal, J., Dupuy, C. (1987) Geochemistry of amphibole pyroxenite veins from the Lherz and Freychinede ultramafic bodies (Ariege, French Pyrenees). Bulletin de minéralogie, 110, 345-358.

611 Boettcher, A., O'Neil, J. (1980) Stable isotope, chemical, and petrographic studies of high-
612 pressure amphiboles and micas: evidence for metasomatism in the mantle source regions
613 of alkali basalts and kimberlites. American Journal of Science, 280, 594-621.

614 Bonadiman, C,. Nazzareni, S., Coltorti ,M., Comodi, P., Giuli, G., Faccin,i B. (2014) Crystal
615 chemistry of amphiboles: implications for oxygen fugacity and water activity in
616 lithospheric mantle beneath Victoria Land, Antarctica. Contributions to Mineralogy
617 Petrology, 167, 984.

618 Chalot-Prat, F., Boullier, A.-M. (1997) Metasomatism in the subcontinental mantle beneath the
619 Eastern Carpathians (Romania): new evidence from trace element geochemistry.
620 Contributions to Mineralogy Petrology, 129, 284-307.

621 Coltorti, M., Beccaluva, L., Bonadiman, C., Faccin,i B., Ntaflos, T., Siena, F. (2004) Amphibole
622 genesis via metasomatic reaction with clinopyroxene in mantle xenoliths from Victoria
623 Land, Antarctica. Lithos, 75, 115-139.

624 Coltorti, M., Bonadiman, C., Faccini, B., Grégoire, M., O'Reilly, S.Y., Powell, W. (2007)
625 Amphiboles from suprasubduction and intraplate lithospheric mantle. Lithos, 99, 68-84.

626 Crépisson, C., Blanchard, M., Bureau, H., Sanloup, C., Withers, A.C., Khodja, H., Surblé, S.,
627 Raepsaet, C., Béneut, K., Leroy, C. (2014) Clumped fluoride-hydroxyl defects in
628 forsterite: Implications for the upper-mantle. Earth Planetary Science Letters, 390, 287-
629 295.

630 Dahlgren, S. (1994) Late Proterozoic and Carboniferous ultramafic magmatism of carbonatitic
631 affinity in southern Norway. 31, 141-154.

632 Dawson, J., Smith, J. (1982) Upper-mantle amphiboles: a review. Mineralogical Magazine, 45,
633 35-46.

634 Dawson, J., Smith, J. (1988) Metasomatised and veined upper-mantle xenoliths from Pello Hill,

635 Tanzania: evidence for anomalously-light mantle beneath the Tanzanian sector of the East
636 African Rift Valley. Contributions to Mineralogy Petrology ,100, 510-527.

637 Dawson, J. (1992) Neogene tectonics and volcanicity in the North Tanzania sector of the Gregory
638 Rift Valley: contrasts with the Kenya sector. Tectonophysics, 204, 81-92.

639 Dawson, J., Smith ,J. (1992) Olivine-mica pyroxenite xenoliths from northern Tanzania:
640 metasomatic products of upper-mantle peridotite. Journal of Volcanology Geothermal
641 Research, 50, 131-142.

642 Debret, B., Koga, K.T., Nicollet, C., Andreani, M., Schwartz, S. (2014) F, Cl and S input via
643 serpentinite in subduction zones: implications for the nature of the fluid released at depth.
644 Terra Nova, 26, 96-101.

645 Dèzes, P., Schmid, S., Ziegler, P. (2004) Evolution of the European Cenozoic Rift System:
646 interaction of the Alpine and Pyrenean orogens with their foreland lithosphere.
647 Tectonophysics, 389, 1-33.

648 Dingwell, D.B., Mysen, B.O. (1985) Effects of water and fluorine on the viscosity of albite melt at
649 high pressure: a preliminary investigation. Earth Planetary Science Letters, 74, 266-274.

650 Douce, A.E.P., Roden, M.F., Chaumba, J., Fleisher, C., Yogodzinski, G. (2011) Compositional
651 variability of terrestrial mantle apatites, thermodynamic modeling of apatite volatile
652 contents, and the halogen and water budgets of planetary mantles. Chemical Geology, 288,
653 14-31.

654 Ebinger, C.J., Sleep, N. (1998) Cenozoic magmatism throughout east Africa resulting from impact
655 of a single plume. Nature, 395, 788.

656 Exley, R., Sills, J., Smith, J. (1982) Geochemistry of micas from the Finero spinel-lherzolite,
657 Italian Alps. Contributions to Mineralogy Petrology, 81, 59-63.

658 Fabbrizio, A., Stalder, R., Hametner, K., Günther, D., Marquardt, K. (2013) Experimental

659 partitioning of halogens and other trace elements between olivine, pyroxenes, amphibole
660 and aqueous fluid at 2 GPa and 900–1,300 C. Contributions to Mineralogy Petrology, 166,
661 639-653.

662 Frey, F.A,. Prinz, M. (1978) Ultramafic inclusions from San Carlos, Arizona, petrologic and
663 geochemical data bearing on their petrogenesis. Earth Planetary Science Letters, 38, 129-
664 176.

665 Frezzotti, M.L., Ferrando, S. (2018) The role of halogens in the lithospheric mantle. The Role of
666 Halogens in Terrestrial and Extraterrestrial Geochemical Processes. Springer, pp 805-846.

667 Gervasoni, F., Klemme, S., Rohrbach, A., Grützner, T., Berndt, J. (2017) Experimental constraints
668 on mantle metasomatism caused by silicate and carbonate melts. Lithos, 282, 173-186.

669 Giovanardi, T., Mazzucchelli, M., Zanetti, A., Langone, A., Tiepolo, M., Ciproani, A. (2014)
670 Occurrence of phlogopite in the finero Mafic Layered Complex. European journal of
671 Geosciences, 6, 588-613.

672 Giuliani, A., Phillips, D., Kamenetsky, V.S., Goemann, K. (2016) Constraints on kimberlite ascent
673 mechanisms revealed by phlogopite compositions in kimberlites and mantle xenoliths.
674 Lithos, 240, 189-201.

675 Goncharov, A., Nikitina, L., Borovkov, N., Babushkina, M., Sirotkin, A . (2015) Thermal and
676 redox equilibrium conditions of the upper-mantle xenoliths from the Quaternary volcanoes
677 of NW Spitsbergen, Svalbard Archipelago. Russian Geology Geophysics, 56, 1578-1602.

678 González-Jiménez, J.M., Villaseca, C., Griffin, W.L., O'Reilly, S.Y., Belousova, E., Ancochea E.,
679 Pearson N.J. (2014) Significance of ancient sulfide PGE and Re–Os signatures in the
680 mantle beneath Calatrava, Central Spain. Contributions to Mineralogy Petrology 168,
681 1047.

682 Griffin, W., Nikolic, N., O'Reilly, S.Y., Pearson, N. (2012) Coupling, decoupling and

683 metasomatism: evolution of crust–mantle relationships beneath NW Spitsbergen. Lithos,
684 149, 115-135.

685 Griffin, W.L. (1973) Lherzolite nodules from the Fen alkaline complex, Norway. Contributions to
686 Mineralogy Petrology, 38, 135-146.

687 Grützner, T., Kohn, S.C., Bromiley, D.W., Rohrbach, A., Berndt, J., Klemme, S. (2017) The
688 storage capacity of fluorine in olivine and pyroxene under upper mantle conditions.
689 Geochimica et Cosmochimica Acta, 208, 160-170.

690 Halick, M. (2010) Documenting multiple metasomatic events within the Finero phlogopite
691 peridotite using chlorine isotopes, Ivrea zone, Italy. The University of New Mexico
692 Albuquerque, New Mexico.

693 Hartmann, G., Wedepohl, K.H. (1993) The composition of peridotite tectonites from the Ivrea
694 Complex, northern Italy: residues from melt extraction. Geochimica et Cosmochimica
695 Acta, 57, 1761-1782.

696 Hawthorne, F.C., Oberti, R., Harlow, G.E., Maresch, W.V., Martin, R.F., Schumacher, J.C.,
697 Welch, M.D. (2012) Nomenclature of the amphibole supergroup. American Mineralogist,
698 97, 2031-2048.

699 Hattori, K.H., Guillot, S. (2003) Volcanic fronts form as a consequence of serpentinite
700 dehydration in the forearc mantle wedge. Geology, 31, 525–528.

701 Humphreys, E., Bailey, K., Wall, F., Hawkesworth, C., Kearns, S. (2008) Highly heterogeneous
702 mantle sampled by rapidly erupted carbonate volcanism 9th International Kimberlite
703 Conference Extended Abstract. pp 00255.

704 Ionov, D.A., Griffin, W.L., O'Reilly, S.Y. (1997) Volatile-bearing minerals and lithophile trace
705 elements in the upper mantle. Chemical Geology, 141, 153-184.

706 Ionov, D.A., Bodinier, J.-l., Mukasa, S.B., Zanetti, A. (2002) Mechanisms and sources of mantle

metasomatism, major and trace element compositions of peridotite xenoliths from Spitsbergen in the context of numerical modelling. Journal of Petrology, 43, 2219-2259.

Irving, A.J., Frey, F.A. (1984) Trace element abundances in megacrysts and their host basalts: constraints on partition coefficients and megacryst genesis. Geochimica et Cosmochimica Acta, 48, 1201-1221.

John, T., Scambelluri, M., Frische, M,. Barnes, J.D., Bach, W. (2011) Dehydration of subducting serpentinite: implications for halogen mobility in subduction zones and the deep halogen cycle. Earth Planetary Science Letters, 308, 65-76.

Jones, A., Kostoula, T., Stoppa, F., Woolley, A. (2000) Petrography and mineral chemistry of mantle xenoliths in a carbonate-rich melilititic tuff from Mt. Vulture volcano, southern Italy. Mineralogical Magazine, 64, 593-613.

Kendrick, M. (2018) Halogens in Seawater, Marine Sediments and the Altered Oceanic Lithosphere. The Role of Halogens in Terrestrial and Extraterrestrial Geochemical Processes. Springer, pp 591-648.

Kendrick, M., Hémond, C., Kamenetsky, V., Danyushevsky, L., Devey, C.W., Rodemann, T., Jackson, M., Perfit, M. (2017) Seawater cycled throughout Earth's mantle in partially serpentinized lithosphere. Nature Geoscience, 10, 222.

Kendrick, M.A., Arculus, R.J., Danyushevsky, L.V., Kamenetsky, V.S., Woodhead, J.D., Honda, M. (2014) Subduction-related halogens (Cl, Br and I) and H_2O in magmatic glasses from Southwest Pacific Backarc Basins. Earth Planetary Science Letters, 400, 165-176.

Kendrick, M.A., Scambelluri, M., Honda, M., Phillips, D. (2011) High abundances of noble gas and chlorine delivered to the mantle by serpentinite subduction. Nature Geoscience, 4, 807.

Keyser, M., Ritter, J.R., Jordan, M. (2002) 3D shear-wave velocity structure of the Eifel plume, Germany. Earth Planetary Science Letters, 203, 59-82.

731 Klaudius, J., Keller, J. (2006) Peralkaline silicate lavas at Oldoinyo Lengai, Tanzania. Lithos, 91,
732 173-190.

733 Klemme, S., Stalder, R. (2018) Halogens in the Earth's mantle: what we know and what we don't.
734 The Role of Halogens in Terrestrial and Extraterrestrial Geochemical Processes. Springer,
735 pp 847-869.

736 Köhler, J., Schönenberger, J., Upton, B., Markl, G. (2009) Halogen and trace-element chemistry in
737 the Gardar Province, South Greenland: subduction-related mantle metasomatism and fluid
738 exsolution from alkalic melts. Lithos, 113, 731-747.

739 Kramm, U., Kogarko, L., Kononova, V., Vartiainen, H. (1993) The Kola Alkaline Province of the
740 CIS and Finland: Precise Rb-Sr ages define 380–360 Ma age range for all magmatism.
741 Lithos, 30, 33-44.

742 Kroner, U., Romer, R. (2013) Two plates - many subduction zones: the Variscan orogeny
743 reconsidered. Gondwana Research, 24, 298-329.

744 Kusebauch, C., John, T., Barnes, J.D., Klügel, A., Austrheim, H.O. (2015) Halogen element and
745 stable chlorine isotope fractionation caused by fluid–rock interaction (Bamble Sector, SE
746 Norway). Journal of Petrology, 56, 299-324.

747 Lavecchia, G., Creati, N., Boncio, P. (2002) The intramontane ultra-alkaline Province (IUP) of
748 Italy: a brief review with considerations on the thickness of the underlying lithosphere.
749 Bollettino della Società Geologica Italiana, 1, 87-98.

750 Lee, C., Rudnick, R. (1999) Compositionally stratified cratonic lithosphere: petrology and
751 geochemistry of peridotite xenoliths from the Labait tuff cone, Tanzania Proceedings of
752 the 7th international Kimberlite conference. Red Roof Design Cape Town, pp 503-521.

753 Leger, A., Rebbert, C., Webster, J. (1996) Cl-rich biotite and amphibole from Black Rock forest,
754 Cornwall, New York. Mineralogical Society of America.

755 Locock, A. (2014) An Excel spreadsheet to classify chemical analyses of amphiboles following
756 the IMA 2012 recommendations. Computers & Geosciences, 62, 1-11.

757 López-Ruiz, J., Cebriá, J., Doblas, M., Oyarzun, R., Hoyos, M., Martín, C. (1993) Cenozoic intra-
758 plate volcanism related to extensional tectonics at Calatrava, central Iberia. Journal of the
759 Geological Society, 150, 915-922.

760 Markl, G., Bucher, K. (1998) Composition of fluids in the lower crust inferred from metamorphic
761 salt in lower crustal rocks. Nature, 391, 781.

762 Marschall, H.R., Altherr, R., Gméling, K., Kasztovszky, Z. (2009) Lithium, boron and chlorine as
763 tracers for metasomatism in high-pressure metamorphic rocks: a case study from Syros
764 (Greece). Mineralogy Petrology, 95, 291.

765 Matusiak-Małek, M., Ćwiek, M., Puziewicz, J., Ntaflos, T. (2017a) Thermal and metasomatic
766 rejuvenation and dunitization in lithospheric mantle beneath Central Europe–The Grodziec
767 (SW Poland) case study. Lithos, 276, 15-29.

768 Matusiak-Małek, M., Puziewicz, J., Ntaflos, T., Grégoire, M., Kukuła, A., Wojtulek, P.M. (2017b)
769 Origin and evolution of rare amphibole-bearing mantle peridotites from Wilcza Góra (SW
770 Poland), Central Europe. Lithos, 286, 302-323.

771 Mayer, B., Jung, S., Romer, R., Pfänder, J., Klügel, A., Pack, A., Gröne,r E. (2014) Amphibole in
772 alkaline basalts from intraplate settings: implications for the petrogenesis of alkaline lavas
773 from the metasomatised lithospheric mantle. Contributions to Mineralogy Petrology, 167,
774 989.

775 Morishita, T., Arai, S., Tamura, A. (2003) Petrology of an apatite-rich layer in the Finero
776 phlogopite–peridotite, Italian Western Alps; implications for evolution of a
777 metasomatising agent. Lithos, 69, 37-49.

778 Morishita, T., Hattori, K.H., Terada, K., Matsumoto, T., Yamamoto, K., Takebe, M., Ishida, Y.,

779 Tamura, A., Arai, S. (2008) Geochemistry of apatite-rich layers in the Finero phlogopite–
780 peridotite massif (Italian Western Alps) and ion microprobe dating of apatite. Chemical
781 Geology, 251, 99-111.

782 Mosenfelder, J.L., Rossman, G.R. (2013a) Analysis of hydrogen and fluorine in pyroxenes: I.
783 Orthopyroxene. American Mineralogist, 98, 1026-1041.

784 Mosenfelder, J.L., Rossman, G.R. (2013b) Analysis of hydrogen and fluorine in pyroxenes: II.
785 Clinopyroxene. American Mineralogist 98, 1042-1054.

786 Munoz, J. (1984) ll. F-OH and Cl-OH Exchange in Micas with applications to hydrothermal ore
787 deposits. 13, 469-493.

788 O'Reilly, S.Y., Griffin, W. (2000) Apatite in the mantle: implications for metasomatic processes
789 and high heat production in Phanerozoic mantle. Lithos, 53, 217-232.

790 Orberger, B., Metrich, N., Mosbah, M., Mével, C., Fouquet, Y. (1999) Nuclear microprobe
791 analysis of serpentine from the mid-Atlantic ridge. Nuclear Instruments Methods in
792 Physics Research Section B: beam Interactions with Materials Atoms, 158, 575-581.

793 Pagé, L., Hattori, K., de Hoog, J.C., Okay, A.I. (2016) Halogen (F, Cl, Br, I) behaviour in
794 subducting slabs: a study of lawsonite blueschists in western Turkey. Earth Planetary
795 Science Letters ,442, 133-142.

796 Pagé, L., Hattori, K. (2017) Tracing halogen and B cycling in subduction zones based on
797 obducted, subducted and forearc serpentinites of the Dominican Republic. Scientific
798 reports ,7,17776.

799 Pagé, L., Hattori, K. (2019) Abyssal Serpentinites: Transporting Halogens from Earth's Surface to
800 the Deep Mantle. Minerals, 9,61.

801 Pearson, D., Davies, G., Nixon, P. (1993) Geochemical constraints on the petrogenesis of diamond
802 facies pyroxenites from the Beni Bousera peridotite massif, North Morocco. Journal of

803 Petrology, 34, 125-172.

804 Pilet, S., Baker, M.B., Stolper, E.M. (2008) Metasomatized lithosphere and the origin of alkaline
805 lavas. Science, 320, 916-919.

806 Reguir, E., Chakhmouradian, A., Halden, N., Malkovets, V., Yang, P. (2009) Major-and trace-
807 element compositional variation of phlogopite from kimberlites and carbonatites as a
808 petrogenetic indicator. Lithos, 112, 372-384.

809 Rehfeldt, T., Foley, S.F., Jacob, D.E., Carlson, R.W., Lowry, D. (2008) Contrasting types of
810 metasomatism in dunite, wehrlite and websterite xenoliths from Kimberley, South Africa.
811 Geochimica et Cosmochimica Acta, 72, 5722-5756.

812 Ritter, J.R., Jordan, M., Christensen, U.R., Achauer, U. (2001) A mantle plume below the Eifel
813 volcanic fields, Germany. Earth Planetary Science Letters, 186, 7-14.

814 Robert, J.-L., Ventura, G.D., Hawthorne, F.C. (1999) Near-infrared study of short-range disorder
815 of OH and F in monoclinic amphiboles. American Mineralogist, 84, 86-91.

816 Rosatelli, G., Stoppa, F., Jones, A. (2000) Intrusive calcite-carbonatite occurrence from Mt.
817 Vulture volcano, southern Italy. De Gruyter.

818 Rosatelli, G., Wall, F., Stoppa, F. (2007) Calcio-carbonatite melts and metasomatism in the mantle
819 beneath Mt. Vulture (Southern Italy). Lithos, 99, 229-248.

820 Rosenbaum J.M. (1993) Mantle phlogopite: a significant lead repository? Chemical Geology, 106,
821 475-483.

822 Rudnick, R., McDonough, W.F., Chappell, B.W. (1993) Carbonatite metasomatism in the
823 northern Tanzanian mantle: petrographic and geochemical characteristics. Earth and
824 Planetary Sceince Letters, 114, 463-475.

825 Rudnick R., McDonough, W.F., Orpin, A. (1994) Northern Tanzanian peridotite xenolith: a
826 comparison with Kaapvaal peridotites and evidence for carbonatite interaction with ultra-

refractory residues Proc 5th Int'l Kimberlite conference. CPRM, pp 336-353.

Rüpke L.H., Morgan J.P., Hort M., Connolly J.A .(2002) Are the regional variations in Central American arc lavas due to differing basaltic versus peridotitic slab sources of fluids? Geology, 30, 1035-1038.

Schmincke, H.-U., Lorenz, V., Seck, H. (1983) The quaternary Eifel volcanic fields Plateau uplift. Springer, pp 139-151.

Selverstone, J., Sharp, Z.D. (2011) Chlorine isotope evidence for multicomponent mantle metasomatism in the Ivrea Zone. Earth Planetary Science Letters, 310, 429-440.

Shaw, C.S., Eyzaguirre, J. (2000) Origin of megacrysts in the mafic alkaline lavas of the West Eifel volcanic field, Germany. Lithos, 50, 75-95.

Sinigoi, S., Comin-Chiaramonti, P., Demarchi, G., Siena, F. (1983) Differentiation of partial melts in the mantle: evidence from the Balmuccia peridotite, Italy. Contributions to Mineralogy Petrology, 82, 351-359.

Smith ,J. (1981) Halogen and phosphorus storage in the Earth. Nature, 289, 762.

Smith, J., Delaney, J., Hervig, R., Dawson, J. (1981) Storage of F and Cl in the upper mantle: geochemical implications. Lithos, 14, 133-147.

Soto, E.A., Giuliani, A. (1979) Edades radiométricas K-Ar del vulcanismo de la región central española. Estudios geológicos, 35, 131-135.

Stosch, H.-G., Seck, H. (1980) Geochemistry and mineralogy of two spinel peridotite suites from Dreiser Weiher, West Germany. Geochimica et Cosmochimica Acta, 44, 457-470.

Straub, S.M., Layne, G.D. (2003) The systematics of chlorine, fluorine, and water in Izu arc front volcanic rocks: implications for volatile recycling in subduction zones. Geochimica et Cosmochimica Acta, 67, 4179-4203.

Sushchevskaya, N., Evdokimov, A., Belyatsky, B., Maslov, V., Kuz'min, D. (2008) Conditions of quaternary magmatism at Spitsbergen Island. Geochemistry international, 46, 1-16.

Urann, B.M., Le Roux, V., Hammond, K., Marschall, H.R., Lee, C-.T., Monteleone, B. (2017) Fluorine and chlorine in mantle minerals and the halogen budget of the Earth's mantle. Contributions to Mineralogy Petrology, 172, 51.

van Acken, D., Becker, H., Walker, R.J., McDonough, W.F., Wombacher, F., Ash, R.D,. Piccoli P.M. (2010) Formation of pyroxenite layers in the Totalp ultramafic massif (Swiss Alps) – insights from highly siderophile elements and Os isotopes. Geochimica et Cosmochimica Acta, 74, 661-683.

Van den Bleeken, G., Koga, K.T. (2015) Experimentally determined distribution of fluorine and chlorine upon hydrous slab melting, and implications for F–Cl cycling through subduction zones. Geochimica et Cosmochimica Acta, 171, 353-373.

Villaseca, C., Ancochea, E., Orejana, D., Jeffries, T. (2010) Composition and evolution of the lithospheric mantle in central Spain: inferences from peridotite xenoliths from the Cenozoic Calatrava volcanic field. Geological Society, London, Special Publications, 337, 125-151.

Volfinger, M., Robert, J.-L., Vielzeuf, D., Neiva, A. (1985) Structural control of the chlorine content of OH-bearing silicates (micas and amphiboles). Geochimica et Cosmochimica Acta, 49, 37-48.

Witt-Eickschen, G., Kaminsky, W., Kramm, U., Harte, B. (1998) The nature of young vein metasomatism in the lithosphere of the West Eifel (Germany): geochemical and isotopic constraints from composite mantle xenoliths from the Meerfelder Maar. Journal of Petrology, 39, 155-185.

Witt-Eickschen, G., Seck, H., Mezger, K., Eggins, S., Altherr, R. (2003) Lithospheric mantle

874 evolution beneath the Eifel (Germany): constraints from Sr–Nd–Pb isotopes and trace
875 element abundances in spinel peridotite and pyroxenite xenoliths. Journal of Petrology, 44,
876 1077-1095.

877 Wysoczanski, R., Wright, I., Gamble, J.A., Hauri, E., Luhr, J., Eggins, S., Handler, M. (2006)
878 Volatile contents of Kermadec Arc–Havre Trough pillow glasses: fingerprinting slab-
879 derived aqueous fluids in the mantle sources of arc and back-arc lavas. Journal of
880 Volcanology Geothermal Research, 152, 51-73.

881 Zanetti, A., Mazzucchelli, M., Rivalenti, G., Vannucci, R. (1999) The Finero phlogopite-peridotite
882 massif: an example of subduction-related metasomatism. Contributions to Mineralogy
883 Petrology, 134, 107-122.

884 Zinngrebe, E., Foley, S. (1995) Metasomatism in mantle xenoliths from Gees, West Eifel,
885 Germany: evidence for the genesis of calc-alkaline glasses and metasomatic Ca-
886 enrichment. Contributions to Mineralogy Petrology, 122, 79-96.

887

888

889 **FIGURE CAPTIONS**

890 **Fig. 1**: Sample localities from this study.

891 **Fig. 2**: Exemplary microtextures of the studied samples. (a) Harzburgite from Finero (FIN-
892 01) with evenly distributed phlogopite and amphibole. (b) Dunite LB-33 from Labait
893 (Tanzania) with small euhedral phlogopite flakes unevenly distributed throughout the sample.
894 (c) Amphibole-rich veins in a dunite (sample 14649) from Calatrava (Spain). (d) Amphibole
895 in a harzburgite from Eifel (EIF-09), surrounded by breakdown products glass,
896 clinopyroxene, spinel and olivine. (e) Olivine websterite EIF-04 (Eifel) with amphibole and
897 phlogopite enclosing clinopyroxene and patches of interstitial glass. (f) Clinopyroxenite ELD-

898 2009-06-1 from the Eledoi (Tanzania) with texturally coexisting mica and clinopyroxene. (g)
899 Coarse-grained and well-equilibrated amphibole and clinopyroxene in hornblendite SHP-7
900 from Spitzbergen. (h) Hornblendite A1008 from Khibina with blocky and elongated
901 amphibole enclosing abundant apatite and magnetite.

902 **Fig. 3:** Major element composition of micas according to sample type. (a) Classification of
903 micas. (b) SiO_2 [wt.%] vs. Mg# (Mg/[Mg + Fe]). (c) SiO_2 [wt.%] vs. TiO_2 [wt.%]. (d) SiO_2
904 [wt.%] vs. Cr_2O_3 [wt.%].

905 **Fig. 4:** Halogen contents (F and Cl) of micas (a) Halogen contents according to sample type
906 and locality. Note that all F and most Cl contents are well above the respective detection
907 limits of 250 µg/g for F and 40 µg/g for Cl (black bars) and the uncertainties for these data
908 points (15-20 % for F and 10% for Cl, see the section on analytical methods) are smaller than
909 the symbol size. For Cl contents relatively close to the detection limit, uncertainties based on
910 counting statistics are about 40 % at the 100 µg/g level and about 20 % at the 200 µg/g level.
911 No overall correlations between (b) Fe# vs. XF (F/(F+Cl+OH)) or (c) Mg# vs. XCl
912 (Cl/(F+Cl+OH) are visible.

913 **Fig. 5:** Major element composition of amphibole according to sample type. (a) Classification
914 of amphiboles based on the current IMA nomenclature (Hawthorne et al. 2012). (b) SiO_2
915 [wt.%] vs. Mg# (Mg/[Mg + Fe]). (c) SiO_2 [wt.%] vs. TiO_2 [wt.%].

916 **Fig. 6:** Halogen contents (F and Cl) of amphiboles (a) Halogen contents according to sample
917 type and locality. Note that most F and Cl contents are well above the respective detection
918 limits of 250 µg/g for F and 40 µg/g for Cl (black bars) and the uncertainties for these data
919 points (15-20 % for F and 10% for Cl, see the section on analytical methods) are smaller than
920 the symbol size. For Cl contents relatively close to the detection limit, uncertainties based on
921 counting statistics are about 40 % at the 100 µg/g level and about 20 % at the 200 µg/g level.
922 For F contents at the 300-400 µg/g level uncertainties are around 30-50 %. No overall

923 correlations between (b) Fe# vs. XF (F/(F+Cl+OH)) or (c) Mg# vs. XCl (Cl/(F+Cl+OH) are
924 visible.

925 **Fig. 7:** Comparison between Cl and F contents in amphibole and phlogopite from this study
926 and literature data (modified from Klemme and Stalder 2018). References: 1 = Bonadiman et
927 al. (2014), 2 = Irving and Frey (1984), 3 = Smith et al. (1981), 4 = Boettcher and O'Neil
928 (1980), 5 = Bénard et al. (2017), 6 = Giuliani et al. (2016), 7 = Reguir et al. (2009), 8 =
929 Rosenbaum (1993), 9 = Rehfeldt et al. (2008) 10 = (Ionov et al. 1997), 11 = (O'Reilly and
930 Griffin 2000), 12 = (Douce et al. 2011).

931 **Fig. 8:** The desiccation effect causes decreasing F/Cl ratios in amphibole and mica with
932 increasing fluid consumption and Cl enrichment. Possible desiccation trends for the different
933 localities are indicated as curved arrows.

934 **Fig. 9:** Halogen budget for a model peridotite (60% olivine, 20% clinopyroxene, 20%
935 orthopyroxene) with variable amounts of amphibole and phlogopite. The stippled and thick
936 lines indicate the proportion of F and Cl hosted in amphibole and phlogopite. Data for NAMs
937 (olivine, clinopyroxene and orthopyroxene) from Urann et al. (2017).

938

This is a preprint, the final version is subject to change, of the American Mineralogist (MSA)
Cite as Authors (Year) Title. American Mineralogist, in press.
DOI: https://doi.org/10.2138/am-2020-7174

Table 1: List of sample material investigated during this study along with information on the amount of amphibole and mica present and previous publications on the studied samples.

Locality	Sample number	Sample type	Vol. % amphibole	Vol.% mica	Previous publications on these samples
Calatrava (Spain)	10002	Phlogopite vein in dunite	-	>90	Humphreys et al. (2008)
	14649	Amphibole vein in dunite	~90	~10	
	120091	Clinopyroxenite	~10	~5	
	EHW-10903	Megacryst	100	-	
	EHW-12555	Megacryst	100	-	
Khibiny (Russia)	A1008	Hornblendite	>90	~1	Arzamastsev et al. (2005)
	K-1635	Hornblendite	>90	~1	
Labait (Tanzania)	LB-33	Dunite	-	~5	Rudnick et al. (1993); (1994); Lee and Rudnick (1999)
	LB-49	Phlogopite vein in dunite	-	>90	
	89-663	Harzburgite	-	~3	
Eledoi (Tanzania)	ELD-2009-06-1	Clinopyroxenite	-	20-30	None
	ELD-2009-06-2	Clinopyroxenite	-	20-30	
Oldoinyo Lengai (Tanzania)	OL-A-1 & 2	Megacrysts	100	-	None
	OL-P-1,2 & 3	Megacrysts	-	100	
Monte Vulture (Italy)	V-A-3 & 8	Megacrysts	100	-	None
	V-P-1 & 2	Megacrysts	-	100	
Fen (Norway)	FEN-A-1, 2, 3 & 4	Megacrysts	100	-	None
	FEN-P-1, 2 & 3	Megacrysts	-	100	
	FEN-MG	Amphibole+phlogopite aggregate	~50	~50	
	FEN-CG	Amphibole+phlogopite aggregate	~50	~50	
Wilcza Góra (Poland)	WLK30	Lherzolite	~1	-	Matusiak-Małek et al. (2017b)
	MLK33	Harzburgite	~1	-	
	MM110	Wehrlite	~1	-	

This is a preprint, the final version is subject to change, of the American Mineralogist (MSA)
Cite as Authors (Year) Title. American Mineralogist, in press.
DOI: https://doi.org/10.2138/am-2020-7174

Spitsbergen (Norway)	SHP-10	Websterite	~5	-	Goncharov et al. (2015)
	SHP-26	Websterite	~5	-	
	SHP-7	Hornblendite	50-70	.	
Eifel (Germany)	EIF-01	Megacryst	-	100	None
	EIF-02	Olivine websterite	~20	~10	
	EIF-04	Olivine websterite	~20	~5	
	EIF-08	Olivine websterite	~10	~1	
	EIF-09	Harzburgite	~5	-	
Finero (Italy)	FIN-01	Harzburgite	~5	~5	None
	FIN-02	Phlogopite pocket in Harzburgite	-	>90	
	FIN-03	Harzburgite	~5	-	

This is a preprint, the final version is subject to change, of the American Mineralogist (MSA)
Cite as Authors (Year) Title. American Mineralogist, in press.
DOI: https://doi.org/10.2138/am-2020-7174

Table 2: Reference materials, diffraction crystals, counting times and average detection limits for EPMA analyses of amphibole and mica of the present study.

Element	Reference material	Crystal	Counting time	Average detection limit
Si	Diopside	TAP	16	110
Ti	$SrTiO_3$	PETH	16	120
Al	Al_2O_3	TAP	16	80
Cr	Cr metal	LIFH	30	160
Ca	Diopside	PETJ	16	120
Mg	Diopside	TAP	16	75
Fe	Haematite	LIFH	16	250
Mn	Rhodonite	PETJ	16	180
Ba	Barite	PETH	30	240
Na	Albite	TAP	16	70
K	Sanidine	PETJ	16	100
F	Topaz	LDE1	30	250
Cl	Tugtupite	PETH	30	60

This is a preprint, the final version is subject to change, of the American Mineralogist (MSA)
Cite as Authors (Year) Title. American Mineralogist, in press.
DOI: https://doi.org/10.2138/am-2020-7174

Table 3: Representative phlogopite analyses from mantle xenoliths, megacrystals and from hornblendites investigated in this study.

	FIN-01	FIN-02	14649	LB-33	ELD-1	ELD-2	120091-	FEN-MG
wt.%								
SiO_2	41.22	41.13	40.30	38.32	40.74	39.86	38.82	39.55
Al_2O_3	14.71	15.26	15.24	15.89	14.55	14.54	16.37	15.50
TiO_2	0.90	0.92	3.50	6.42	4.74	4.52	5.17	3.93
Cr_2O_3	1.59	1.60	1.29	1.55	0.21	0.18	0.38	0.00
FeO	2.79	3.07	6.05	3.22	6.82	7.26	8.17	8.79
MgO	24.78	24.82	21.20	21.43	21.90	21.39	19.07	20.39
MnO	0.00	0.00	0.03	0.00	0.00	0.00	0.00	0.03
CaO	0.00	0.02	0.06	0.00	0.00	0.03	0.04	0.00
Na_2O	1.37	1.36	1.19	0.96	1.14	1.16	0.69	0.70
K_2O	8.53	8.51	8.55	9.25	9.04	8.81	9.11	9.11
BaO	0.34	0.34	0.42	0.31	0.16	0.23	0.48	0.56
Cl	0.11	0.01	0.04	0.01	0.00	0.02	0.04	0.05
F	0.23	0.33	0.18	1.96	0.51	0.57	0.19	0.19
Total	96.56	97.37	98.06	99.32	99.80	98.56	98.52	98.80
Elements. atoms per formula unit based on 22 oxygen atoms								
Si	5.74	5.69	5.62	5.34	5.61	5.58	5.45	5.55
Al	2.42	2.49	2.50	2.61	2.36	2.40	2.71	2.56
Ti	0.09	0.10	0.37	0.67	0.49	0.48	0.55	0.41
Cr	0.18	0.18	0.14	0.17	0.02	0.02	0.04	0.00
Fe	0.33	0.36	0.71	0.38	0.78	0.85	0.96	1.03
Mg	5.15	5.12	4.40	4.45	4.49	4.46	3.99	4.26
Mn	0.00	0.00	0.00	0.00	0.00	0.00	0.00	0.00
Ca	0.00	0.00	0.01	0.00	0.00	0.00	0.01	0.00
Na	0.37	0.36	0.32	0.26	0.30	0.31	0.19	0.19
K	1.52	1.50	1.52	1.65	1.59	1.57	1.63	1.63
Ba	0.02	0.02	0.02	0.02	0.01	0.01	0.03	0.03
Cl	0.03	0.00	0.01	0.00	0.00	0.00	0.01	0.01
F	0.10	0.14	0.08	0.86	0.22	0.25	0.08	0.09
Cation Sum	15.79	15.80	15.59	15.53	15.65	15.67	15.51	15.64

This is a preprint, the final version is subject to change, of the American Mineralogist (MSA)
Cite as Authors (Year) Title. American Mineralogist, in press.
DOI: https://doi.org/10.2138/am-2020-7174

wt.%	FEN-MG	EIF-02	EIF-04	120091	LB-49	A1008	Ol-P-21	EIF-01	FEN-P-3	V-P-1
SiO_2	39.55	37.28	39.19	38.78	41.2	36.67	39.54	36.98	38.60	38.36
Al_2O_3	15.50	16.74	15.88	16.27	13.1	16.21	15.25	16.59	17.26	18.52
TiO_2	3.93	4.06	4.63	5.39	4.0	4.32	4.66	6.10	4.62	2.17
Cr_2O_3	0.00	0.00	0.36	0.17	0.7	0.00	0.69	0.05	0.05	0.04
FeO	8.79	10.18	7.99	8.36	7.3	12.64	8.30	8.86	7.13	6.25
MgO	20.39	18.85	19.76	18.65	22.0	17.37	20.62	18.57	19.97	21.82
MnO	0.03	0.09	0.06	0.03	0.0	0.11	0.07	0.07	0.03	0.03
CaO	0.00	0.04	0.15	0.05	0.0	0.02	0.00	0.02	0.04	0.05
Na_2O	0.70	0.68	0.73	0.72	0.6	0.68	0.70	0.58	0.72	0.69
K_2O	9.11	9.23	9.42	9.10	9.9	9.01	9.33	9.13	9.37	9.10
BaO	0.56	0.87	0.29	0.32	0.1	1.39	0.26	0.98	0.56	1.23
Cl	0.05	0.02	0.01	0.03	0.0	0.01	0.01	0.02	0.02	0.02
F	0.19	0.24	0.30	0.18	0.4	0.22	0.42	0.26	0.30	0.20
Total	98.80	98.27	98.77	98.04	99.3	98.66	99.84	98.21	98.67	98.46
Elements. atoms per formula unit. based on 22 oxygen atoms										
Si	5.55	5.33	5.49	5.46	5.73	5.31	5.49	5.27	5.39	5.36
Al	2.56	2.82	2.62	2.70	2.15	2.76	2.50	2.78	2.84	3.05
Ti	0.41	0.44	0.49	0.57	0.42	0.47	0.49	0.65	0.49	0.23
Cr	0.00	0.00	0.04	0.02	0.08	0.00	0.08	0.01	0.01	0.00
Fe	1.03	1.22	0.94	0.99	0.85	1.53	0.96	1.06	0.83	0.73
Mg	4.26	4.02	4.13	3.92	4.56	3.75	4.27	3.94	4.16	4.54
Mn	0.00	0.01	0.01	0.00	0.00	0.01	0.01	0.01	0.00	0.00
Ca	0.00	0.01	0.02	0.01	0.00	0.00	0.00	0.00	0.01	0.01
Na	0.19	0.19	0.20	0.20	0.16	0.19	0.19	0.16	0.20	0.19
K	1.63	1.68	1.68	1.64	1.76	1.66	1.65	1.66	1.67	1.62
Ba	0.03	0.05	0.02	0.02	0.00	0.08	0.01	0.05	0.03	0.07
Cl	0.01	0.00	0.00	0.01	0.00	0.00	0.00	0.00	0.01	.00
F	0.09	0.11	0.13	0.08	0.18	0.10	0.18	0.12	0.13	0.09
Cation Sum	15.64	15.71	15.62	15.50	15.70	15.69	15.64	15.54	15.60	15.73

This is a preprint, the final version is subject to change, of the American Mineralogist (MSA)
Cite as Authors (Year) Title. American Mineralogist, in press.
DOI: https://doi.org/10.2138/am-2020-7174

Table 4: Representative amphibole analyses from mantle xenoliths, megacrystals and from hornblendites investigated in this study.

wt.%	EIF-09-	FIN-01	146493	MM110	SHP-10	FEN-MG	120091	SHP-26
SiO_2	43.67	47.07	45.71	43.40	41.74	43.10	42.30	42.05
Al_2O_3	13.99	9.76	10.45	12.72	14.35	12.47	13.37	15.60
TiO_2	0.52	0.59	3.28	1.98	4.44	2.88	3.88	3.35
Cr_2O_3	1.71	2.08	0.07	2.20	0.23	0.00	0.17	0.16
FeO	3.95	3.29	6.03	4.40	10.39	8.20	7.71	9.07
MgO	18.48	19.81	17.83	17.71	13.71	15.83	15.27	14.14
MnO	0.05	0.06	0.10	0.13	0.11	0.06	0.08	0.07
CaO	11.24	11.77	10.33	11.22	10.21	10.87	11.11	10.34
Na_2O	2.29	2.93	3.60	3.01	3.00	2.80	2.49	3.05
K_2O	1.25	0.76	1.20	1.19	1.19	1.66	2.02	1.12
Cl	0.10	0.11	0.04	0.04	0.04	0.05	0.04	0.05
F	0.07	0.12	0.07	0.00	0.00	0.07	0.06	0.00
Total	97.95	98.35	98.70	98.03	99.41	98.00	98.54	99.02
Elements. atoms per formula unit. Calculations based on different cation sums to achieve charge balance								
Si	6.19	6.61	6.48	6.19	5.99	6.23	6.10	6.01
Al	2.34	1.62	1.75	2.14	2.43	2.13	2.27	2.63
Ti	0.06	0.06	0.35	0.21	0.48	0.31	0.42	0.36
Cr	0.19	0.23	0.01	0.25	0.03	0.00	0.02	0.02
Fe^{3+}	0.24	0.20	0.12	0.16	0.20	0.15	0.07	0.19
Fe^{2+}	0.23	0.19	0.59	0.37	1.05	0.84	0.86	0.89
Mg	3.90	4.15	3.77	3.76	2.93	3.41	3.28	3.01
Mn	0.01	0.01	0.01	0.02	0.01	0.01	0.01	0.01
Ca	1.71	1.77	1.57	1.71	1.57	1.68	1.72	1.58
Na	0.80	0.80	0.99	0.83	0.83	0.79	0.70	0.85
K	0.23	0.14	0.22	0.21	0.22	0.31	0.37	0.20
Cl	0.02	0.03	0.01	0.01	0.01	0.01	0.01	0.01
F	0.03	0.05	0.03	0.00	0.00	0.03	0.03	0.00
Cation Sum	15.89	15.77	15.84	15.85	15.73	15.86	15.83	15.74

This is a preprint, the final version is subject to change, of the American Mineralogist (MSA)
Cite as Authors (Year) Title. American Mineralogist, in press.
DOI: https://doi.org/10.2138/am-2020-7174

wt.%	SHP-26	120091	EIF-02-	Lp-02-4	Lp-02-28	K-A1008	FIN-03	Ol-A-2	FEN-A-1	V-A-8
SiO_2	43.14	42.26	39.91	39.83	39.55	40.04	45.19	40.82	41.25	39.17
Al_2O_3	14.83	13.38	14.03	13.74	13.64	14.00	12.57	12.38	15.24	15.36
TiO_2	4.06	3.68	3.68	6.01	5.79	3.34	1.01	3.30	3.21	2.86
Cr_2O_3	0.13	0.41	0.00	0.00	0.03	0.00	1.18	0.02	0.03	0.00
FeO	9.75	7.59	10.27	9.93	10.90	12.37	4.81	11.13	6.50	9.57
MgO	13.51	15.28	14.01	13.56	12.73	12.51	17.94	14.36	15.92	14.68
MnO	0.09	0.07	0.14	0.09	0.14	0.16	0.11	0.13	0.10	0.06
CaO	9.85	11.05	12.22	12.35	12.14	11.58	12.21	11.78	11.62	12.69
Na_2O	2.93	2.47	2.28	2.71	2.82	2.40	2.45	2.67	2.22	2.05
K_2O	1.54	2.04	2.13	1.16	1.17	2.05	0.12	1.66	2.35	2.05
Cl	0.06	0.04	0.03	0.02	0.02	0.02	0.01	0.01	0.02	0.03
F	0.00	0.10	0.10	0.16	0.17	0.08	0.00	0.22	0.14	0.25
Total	99.89	98.36	98.86	99.60	99.09	98.62	97.59	98.54	98.66	98.93
Elements. atoms per formula unit. Calculations based on different cation sums to achieve charge balance										
Si	6.12	6.11	5.85	5.79	5.81	5.93	6.38	6.00	5.93	5.70
Al	2.48	2.28	2.42	2.36	2.36	2.44	2.09	2.14	2.58	2.64
Ti	0.43	0.40	0.41	0.66	0.64	0.37	0.11	0.37	0.35	0.31
Cr	0.02	0.05	0.00	0.00	0.00	0.00	0.13	0.00	0.00	0.00
Fe^{3+}	0.14	0.08	0.15	0.00	0.00	0.10	0.27	0.29	0.11	0.40
Fe^{2+}	1.01	0.84	1.11	1.21	1.34	1.43	0.30	1.08	0.67	0.77
Mg	2.86	3.29	3.06	2.94	2.79	2.76	3.78	3.14	3.41	3.19
Mn	0.01	0.01	0.02	0.01	0.02	0.02	0.01	0.02	0.01	0.01
Ca	1.50	1.71	1.92	1.92	1.91	1.84	1.85	1.85	1.79	1.98
Na	0.81	0.69	0.65	0.76	0.80	0.69	0.67	0.76	0.62	0.58
K	0.28	0.38	0.40	0.22	0.22	0.39	0.02	0.31	0.43	0.38
Cl	0.01	0.01	0.01	0.00	0.00	0.00	0.00	0.00	0.01	0.01
F	0.00	0.05	0.05	0.08	0.08	0.04	0.00	0.10	0.07	0.10
Cation Sum	15.66	15.83	15.98	15.86	15.88	15.97	15.61	15.96	15.90	15.95

This is a preprint, the final version is subject to change, of the American Mineralogist (MSA)
Cite as Authors (Year) Title. American Mineralogist, in press.
DOI: https://doi.org/10.2138/am-2020-7174

Table 5: Halogen contents for olivine, orthopyroxene and clinopyroxene from 17 natural peridotite samples (Urann et al. 2017). For the mass balance calculations performed mean values from this data set abd out own data on amphibole and mica were used.

	Olivine (11 grains); Urann et al. (2017)	**Orthopyroxene** (17 grains); Urann et al. (2017)	**Clinopyroxene** (17 grains); Urann et al. (2017)
F range of mean values [µg/g]	1.7 – 30.5	0.72 – 35.3	0.98 – 83.4
Cl range of mean values [µg/g]	0.15 – 0.34	0.12 – 0.45	0.12 – 0.45
Mean F [µg/g]	6.1	6.9	22.1
Mean Cl [µg/g]	0.22	0.23	0.25

This is a preprint, the final version is subject to change, of the American Mineralogist (MSA)
Cite as Authors (Year) Title. American Mineralogist, in press.
DOI: https://doi.org/10.2138/am-2020-7174

Fig. 1

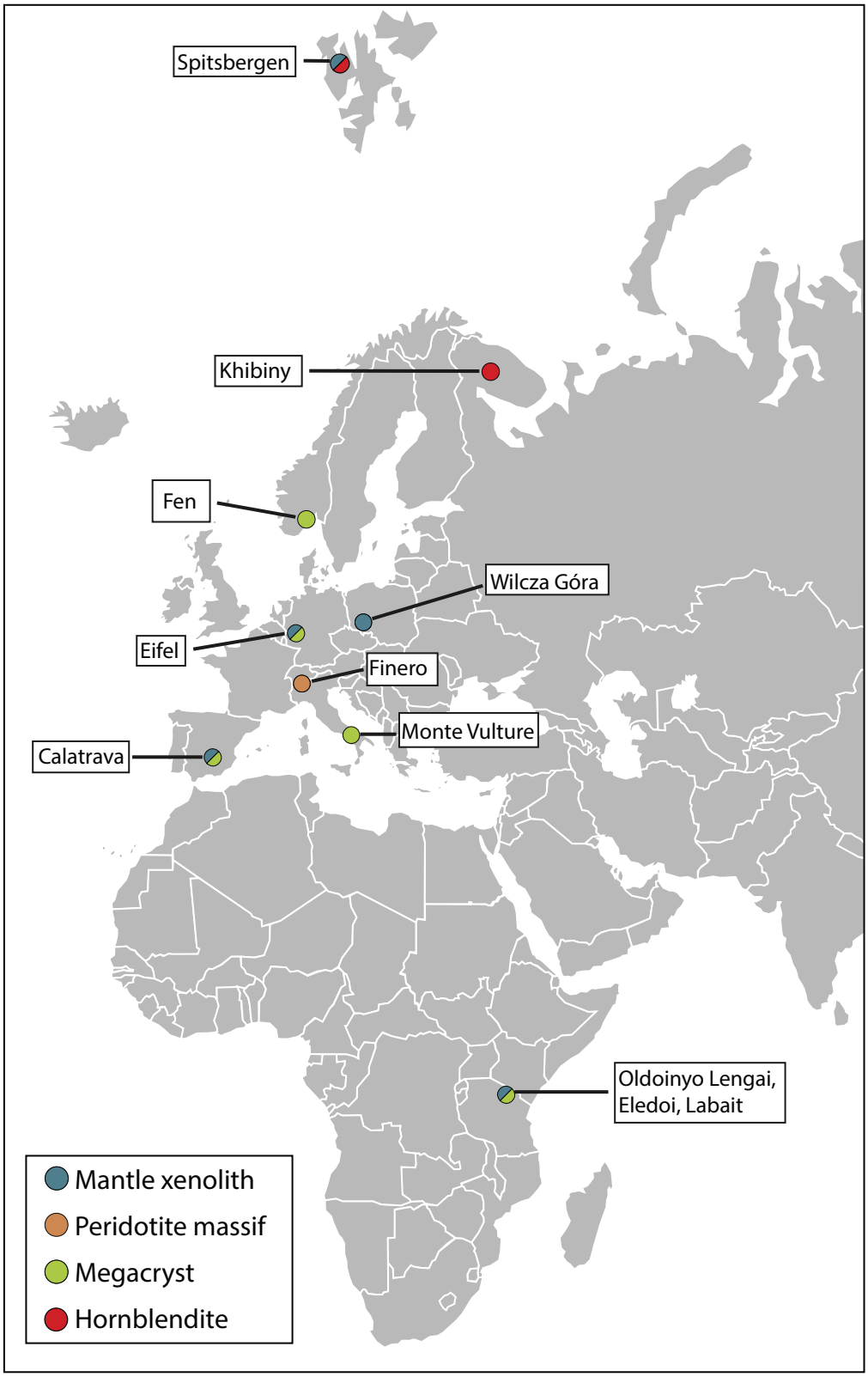

This is a preprint, the final version is subject to change, of the American Mineralogist (MSA)
Cite as Authors (Year) Title. American Mineralogist, in press.
DOI: https://doi.org/10.2138/am-2020-7174

Fig. 2

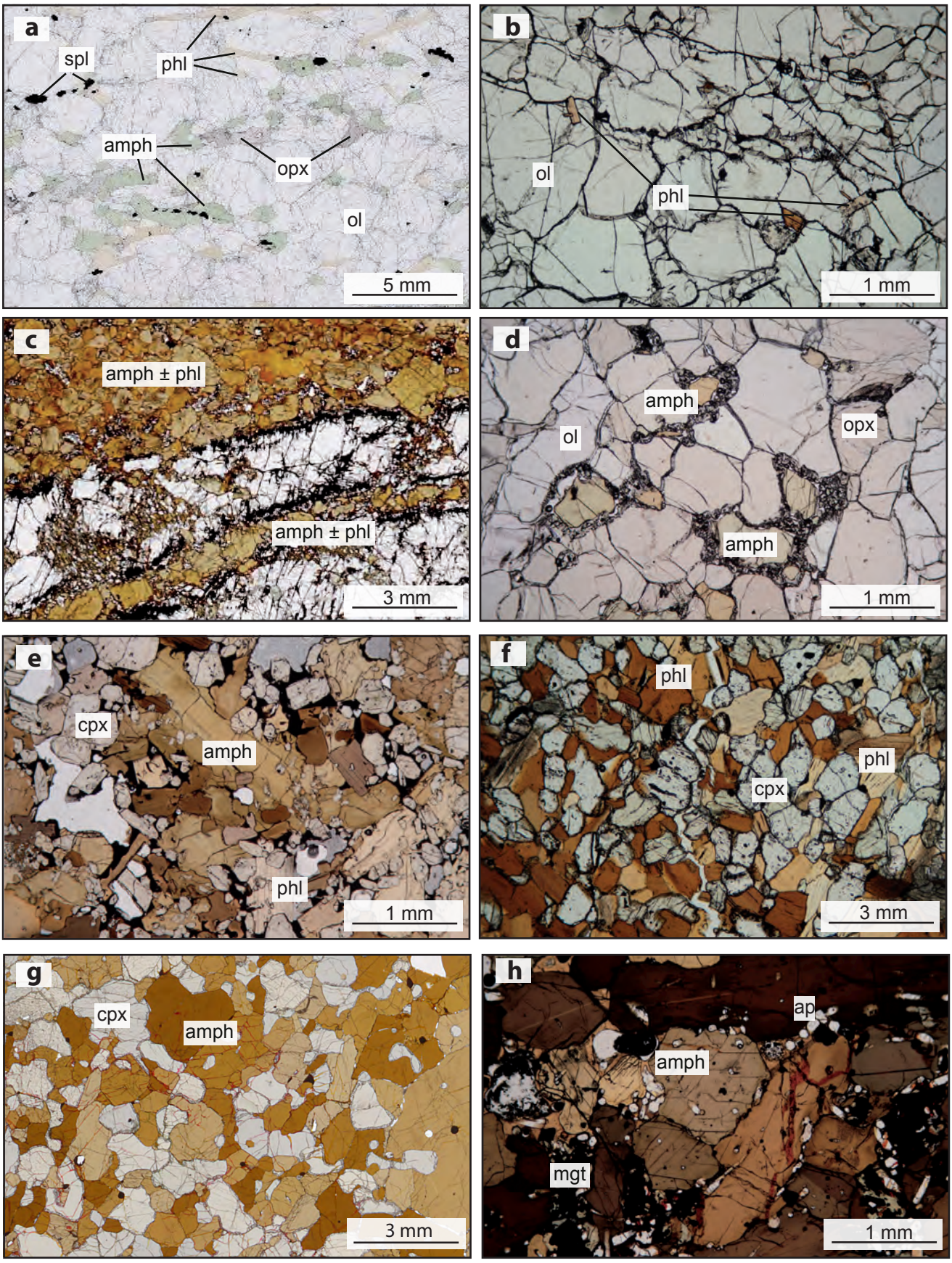

This is a preprint, the final version is subject to change, of the American Mineralogist (MSA)
Cite as Authors (Year) Title. American Mineralogist, in press.
DOI: https://doi.org/10.2138/am-2020-7174

Fig. 3

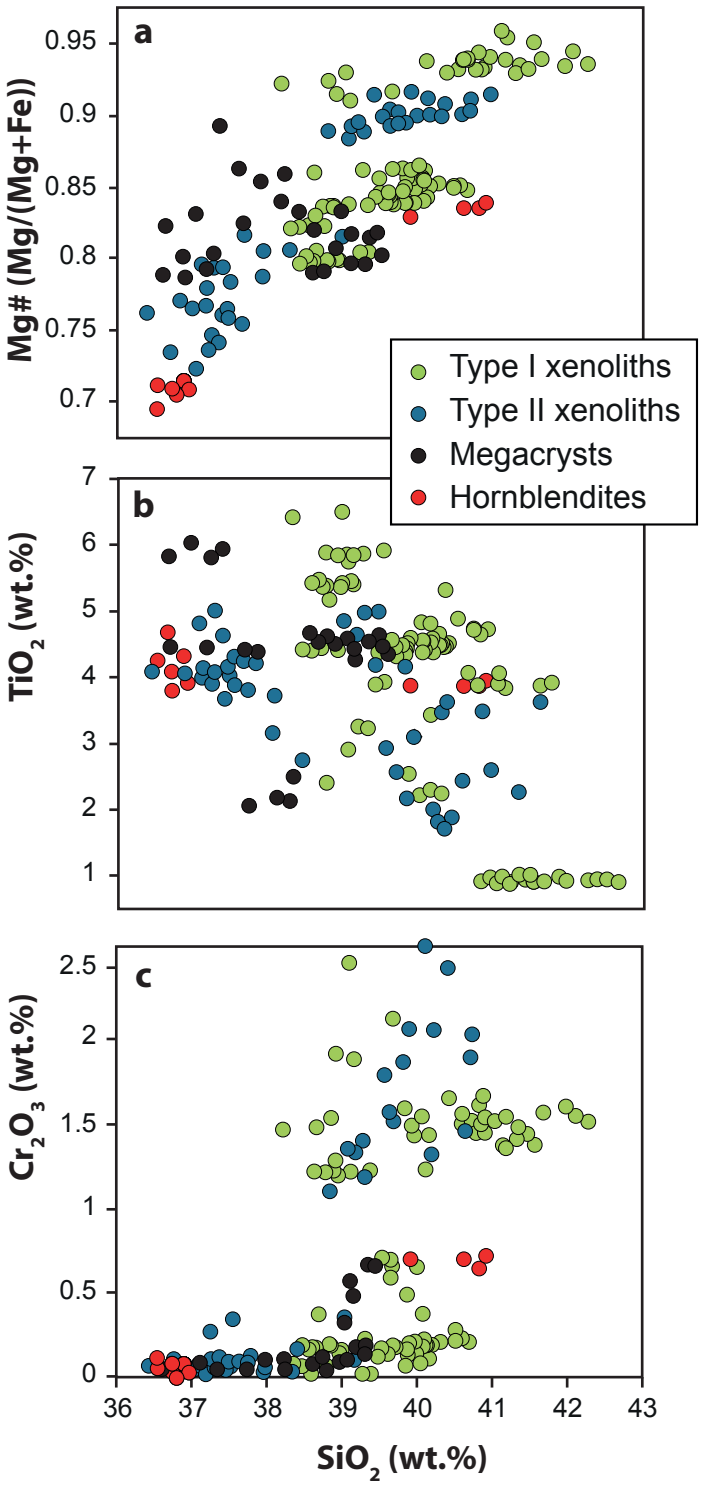

This is a preprint, the final version is subject to change, of the American Mineralogist (MSA)
Cite as Authors (Year) Title. American Mineralogist, in press.
DOI: https://doi.org/10.2138/am-2020-7174

Fig. 4

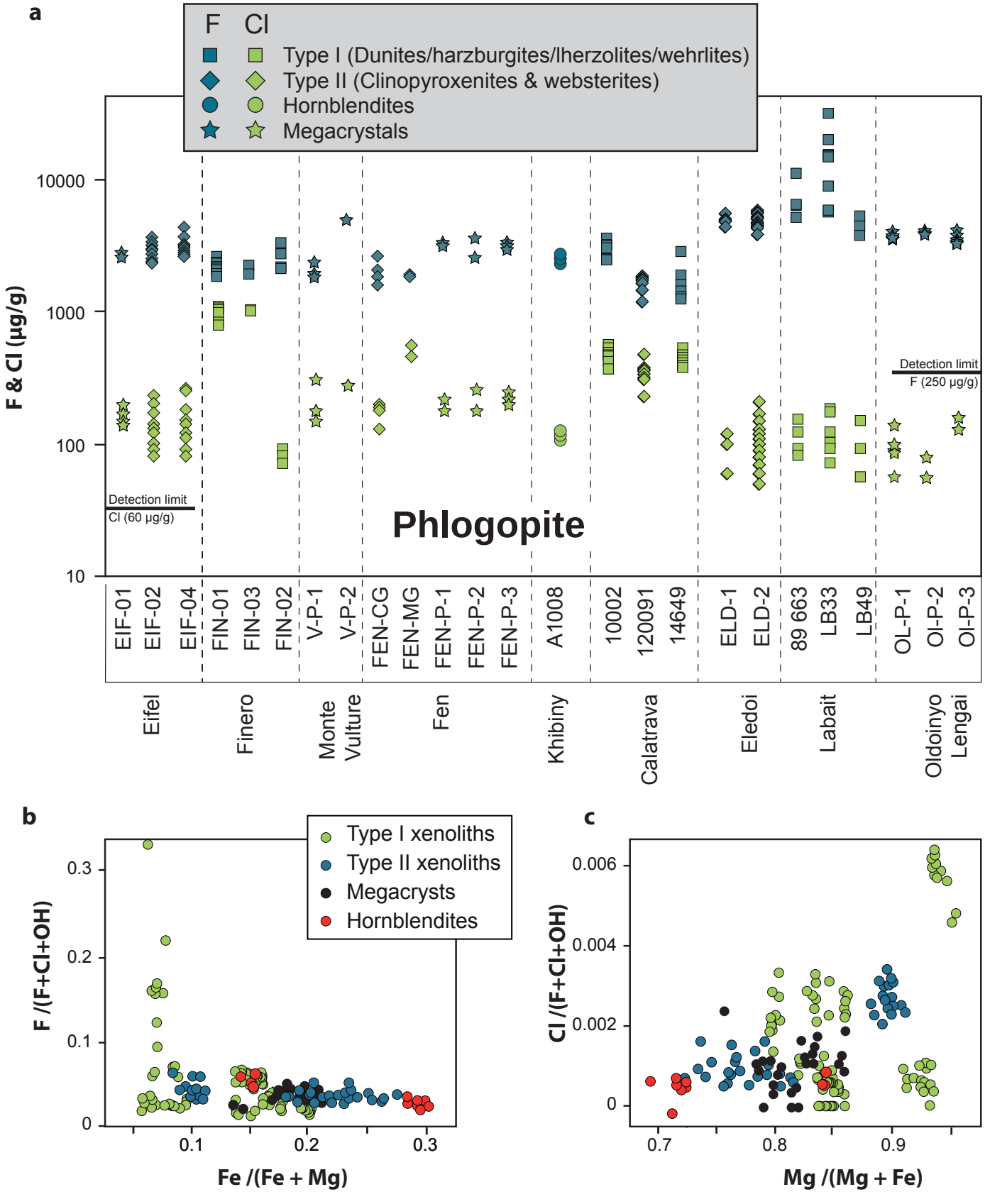

This is a preprint, the final version is subject to change, of the American Mineralogist (MSA)
Cite as Authors (Year) Title. American Mineralogist, in press.
DOI: https://doi.org/10.2138/am-2020-7174

Fig. 5

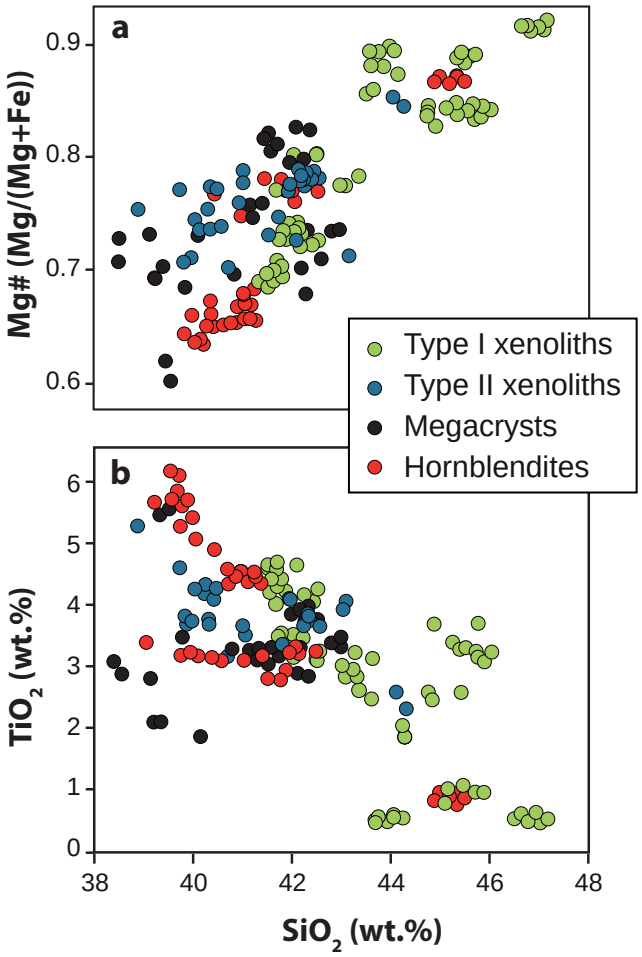

This is a preprint, the final version is subject to change, of the American Mineralogist (MSA)
Cite as Authors (Year) Title. American Mineralogist, in press.
DOI: https://doi.org/10.2138/am-2020-7174

Fig. 6

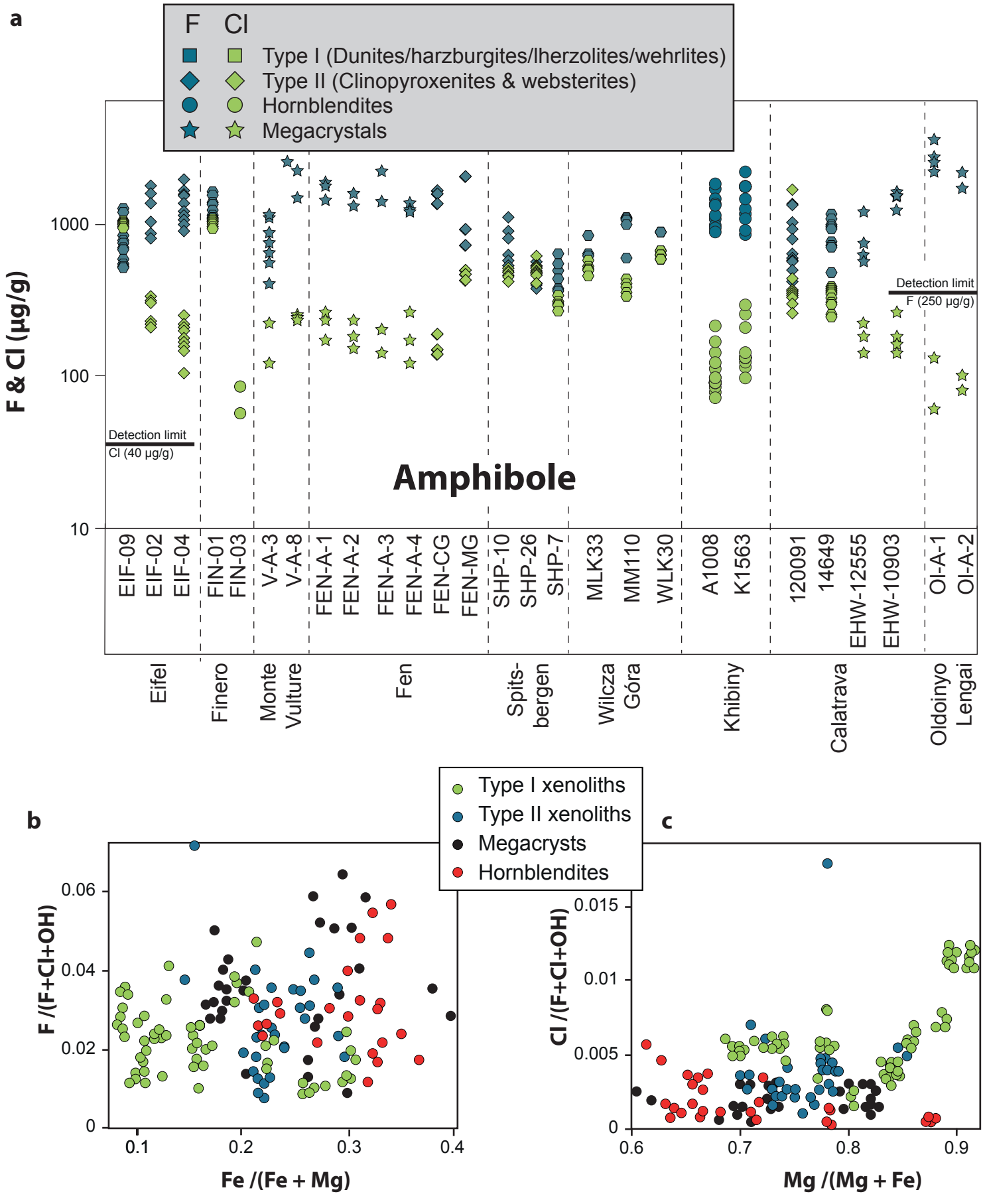

This is a preprint, the final version is subject to change, of the American Mineralogist (MSA)
Cite as Authors (Year) Title. American Mineralogist, in press.
DOI: https://doi.org/10.2138/am-2020-7174

Fig. 7

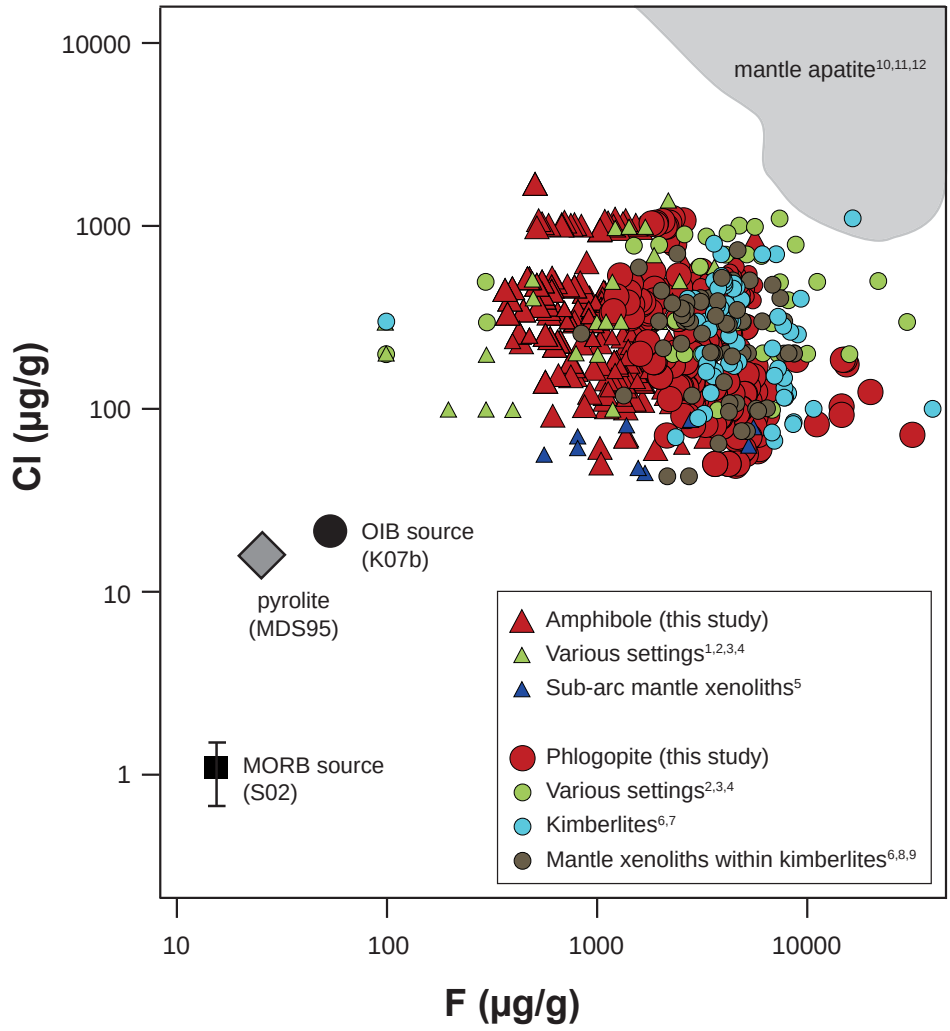

This is a preprint, the final version is subject to change, of the American Mineralogist (MSA)
Cite as Authors (Year) Title. American Mineralogist, in press.
DOI: https://doi.org/10.2138/am-2020-7174

Fig. 8

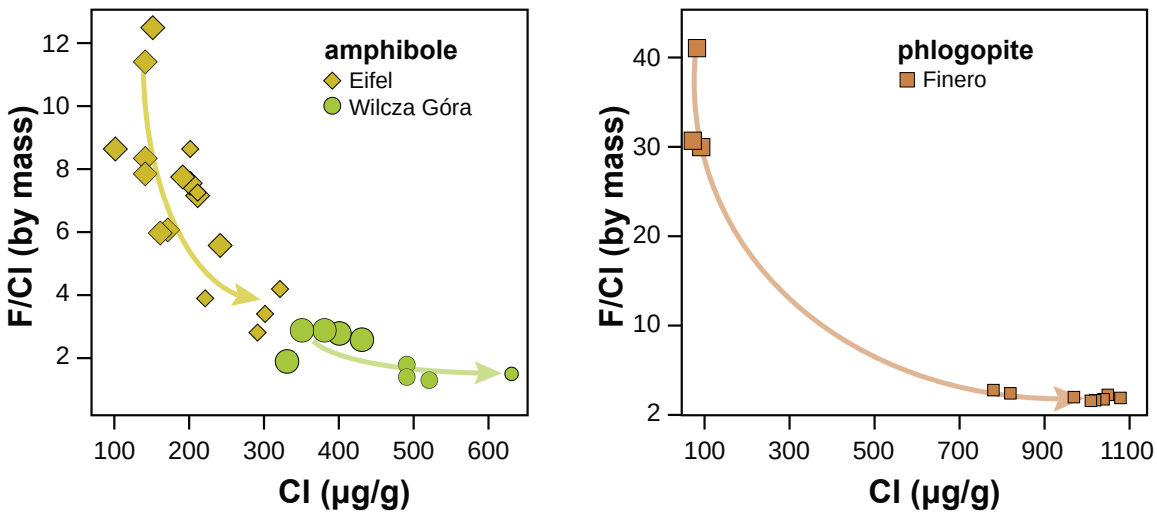

This is a preprint, the final version is subject to change, of the American Mineralogist (MSA)
Cite as Authors (Year) Title. American Mineralogist, in press.
DOI: https://doi.org/10.2138/am-2020-7174

Fig. 9